3

The CE-06 Experimental Apparatus

T he subject of this work, the Cooler ring experiment CE-06, involved the development and construction of equipment designed specifically to take advantage of the physics opportunities afforded by the new accelerator. CE-06 was the first experiment to measure exclusive pion production using a solid target in a storage ring, and represented the first use of heavy recoil ($A > 4$) detection techniques in such a facility. To achieve these goals, a number of experimental challenges had to be met. This chapter describes the Cooler ring facility and the detection apparatus specific to the CE-06 experiment.

3.1   The Cooler Ring

The Indiana University Cyclotron Facility (IUCF) synchotron-storage ring, known in short as the "Cooler," was completed in March, 1988, and the first proton beams were stored a month later. The Cooler represented a new and unique opportunity for nuclear physics: the use of medium-energy light-ion beams of unprecedented brightness and quality. Now, after only a few years of operation, new physics measurements have been made, with an improvement in precision by an order of magnitude in some cases. The elementary pion-production process pp $\rightarrow$ ppπ^0 has been studied in detail [Me90] near threshold to great success, inspiring new theoretical calculations to explain the data [Le93]. A study of s-wave processes in near-threshold pp $\rightarrow$ pnπ^+[Ha93] yielded data closer to threshold (within 2 MeV) than previously accomplished by a factor of 50. The CE-06 experiment
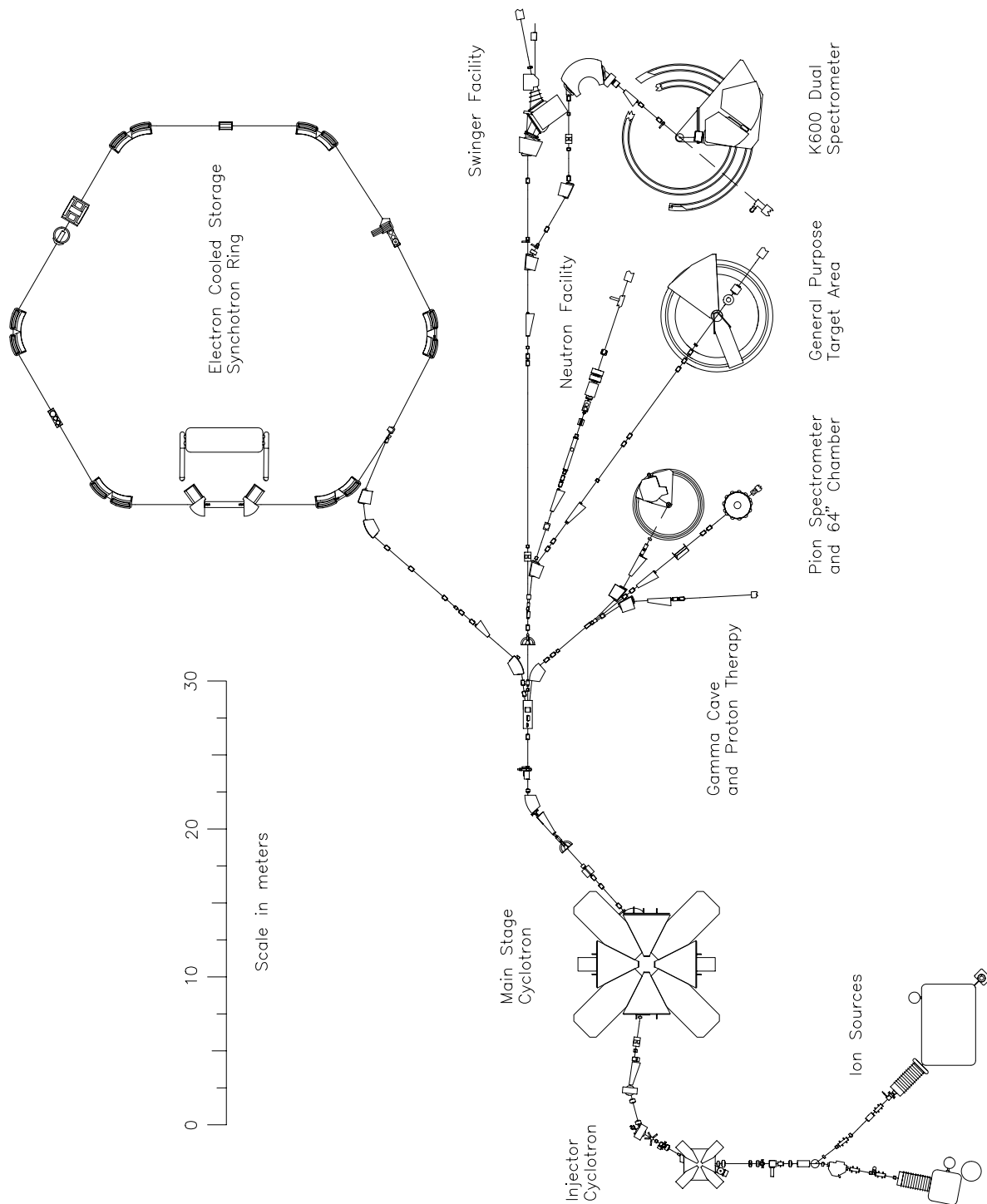
Figure 3.1   Simplified schematic of IUCF, including the injection and main cyclotrons, experimental areas, and Cooler ring. Not shown is the high-intensity polarized ion source to be commissioned in 1993.

was ideally suited to the Cooler, primarily because of the high luminosities possible even with ultra-thin targets.

Figures 3.1 and 3.2 show the Cyclotron Facility and Cooler Ring, respectively, at Indiana University, Bloomington, Indiana. The ion sources can provide both polarized and unpolarized beams of several light-ion species, including H_2^+, He^+, and Li^+. The two-stage accelerator produces proton beams with energies of up to 200 MeV, and services the variety of experimental areas shown in Fig. 3.1. For the CE-06 experiment, the cyclotron facility served as the injection device to the Cooler ring, which can accelerate proton beams to nearly 500 MeV.
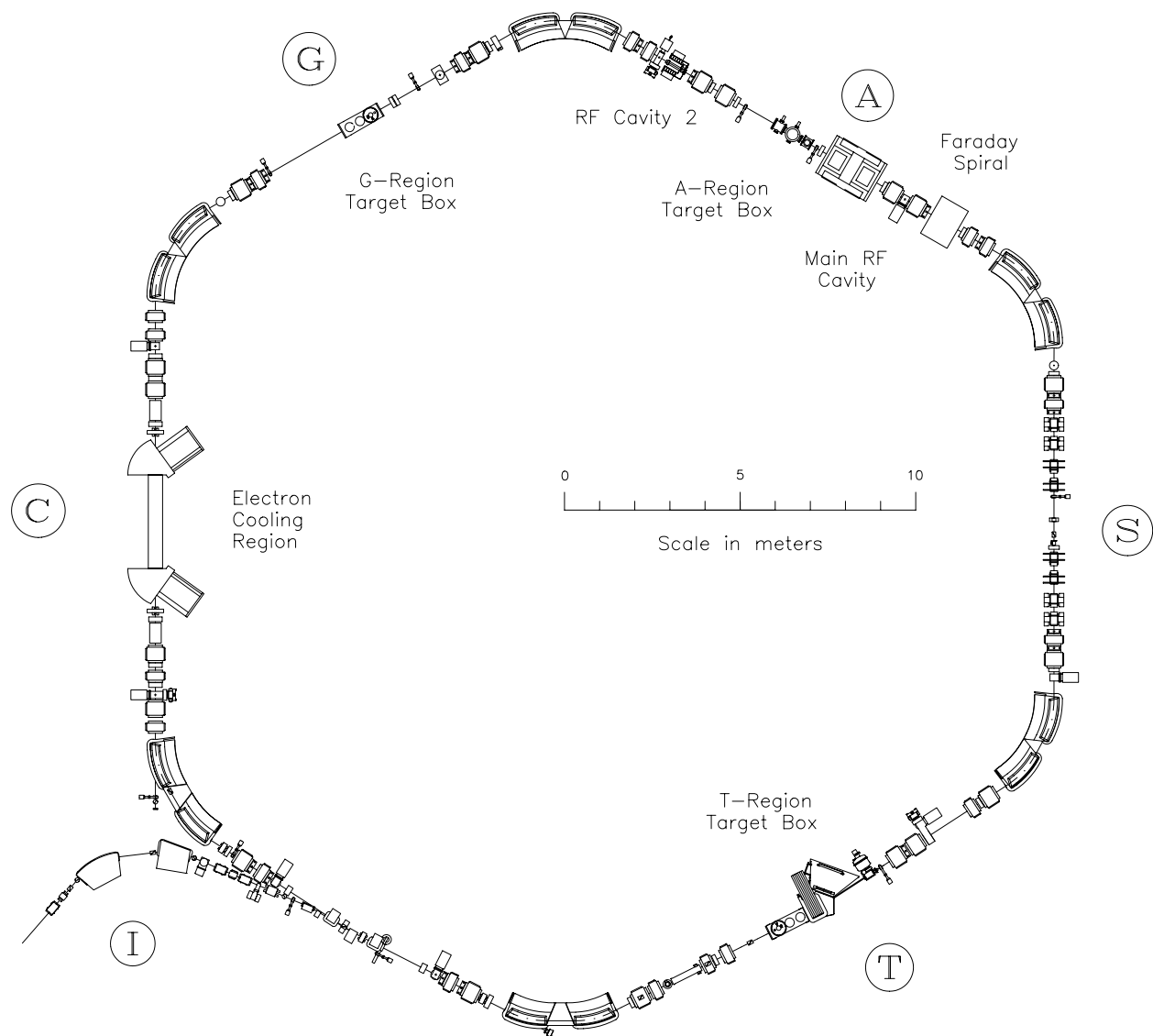

Figure 3.2   The IUCF Cooler ring, with the electron cooling system at the left and the CE-06 location (T-site) at the lower right.

Unlike the main cyclotron and the associated experimental areas, the Cooler is a

storage ring designed for multi-pass experiments using internal targets. Figure 3.2 shows a more detailed drawing of the Cooler. The unusual hexagonal design makes possible a larger number of experimentally accessible straight-sections than in the more typical four-sided "ring." Of the six possible areas, only the cooling system (C) and injection (I) sections are devoted solely to machine operation. The tagged beam (T) and general (G) regions are exclusively for experimental use, whereas the acceleration section (A) not only contains the RF synchotron cavity but has recently been the site of several polarized target experiments [Fr93]. Some important ring parameters are listed in Table 3.1.

	E_p	30–480 MeV
	ΔE_p (300 MeV)	± 100 keV (sys.) ± 20 keV (stat.)
	$(\beta\rho)_{\max}$	3.6 Tesla-meters
General	$L_{\rm ring}$	$86.78 \pm .01$ m
	A_x ($\approx A_y$)	30π mm-mrad
	$\Delta p/p$	$\pm 0.2\%$
	Ramp rate	1 Tesla-meter/sec
	kT_e	0.1–0.2 eV
	I_e	0.5–4 amps
Cooling System	e^- beam diameter	2.5 cm
	$\tau_{\rm cool}$ (300 MeV)	0.5 sec
	longitudinal B field	0.15 Tesla

Table 3.1　　Some characteristic cooler ring parameters.

The centerpiece of the Cooler is its namesake, the electron cooling system. The term "cooling" is used here to describe the increase in phase space density of the circulating ion beam. Equivalently, in a reference frame moving at the beam's average velocity, the cooling can be viewed as a decrease in the width of the ions' velocity distribution, i.e., a reduction of its "temperature." Beam cooling is often very beneficial to experiments for a variety of reasons. First and foremost is the quality of the beam: the small transverse emittance resulting from cooling implies an extremely localized beam profile on target with small halo, and subsequent reduction of background. The compressed longitudinal momentum phase space results in excellent beam energy definition, making possible measurements at closely spaced energies, which is especially important near the threshold of a particular reaction. For example, in the T-region, where the CE-06 experiment was located, a 150 MeV proton

beam on a 100 ng/cm^2 ^{12}C target, typically has [Me88] a diameter of 2 mm, a divergence of less than 1 mrad, and an energy spread (FWHM) of less than 10 keV.[1] In comparison, a 150 MeV proton beam generated by the cyclotron is characterized [Gr83], after momentum selection and collimation in an analyzing magnet, by an energy spread (FWHM) of 160 keV.

Another benefit of cooling is the possibility of running luminosity-limited experiments, for example, measurements of near-threshold and nanobarn-scale cross-sections. A storage ring requires very thin targets ($d_{\mathrm{tgt}} < 100$ ng/cm^2) since the beam is not constantly being replenished as in a single-pass facility. Normally, this would imply luminosities much smaller than that in typical cyclotron experiments. However, the use of cooling enables the storage of very intense beams, yielding large luminosities even with the necessarily thin targets. More than 1 mA of protons have been stored in the Cooler, and luminosities greater than 10^{30} cm^{-2} sec^{-2} have been achieved with both gaseous [Dr91] and solid [this work] targets.

Finally, cooling can greatly increase the storage lifetime of ion beams by counteracting "heating" due to residual beam-line gases or targets, and other destabilizing effects.[2] In the original electron cooling studies [Bu76], the beam lifetime was increased by nearly a factor of 6 compared to a non-cooled beam. Storage times of almost two hours [Po90] have been achieved at the Cooler, with a typical ring vacuum of better than 10^{-8} torr H$_2$ equivalent.

At IUCF, the cooling process is accomplished by accelerating a "cold," intense ($I_e \approx 1$ A) electron beam parallel to the circulating ion beam for a short distance (about 3 meters) in the cooling section (C). The electron energy is tuned to match the ions' average velocity to better than one part in 10^3. In this situation, the cooling process has a quantitative analog in the passage of ions through matter, where the particles lose energy via collisions with atomic electrons, eventually coming to rest in the material. The cooling mechanism is essentially the same process, when viewed from the electrons' rest frame, as long as the electron temperature is much lower than that of the ions.

Equilibrium between the electrons and ions is typically reached in a few hundred msec. This can be accelerated by the strong longitudinal magnetic field commonly used to contain the intense electron beam against its own space charge build-up. The field can also allow the ion beam to be cooled to temperatures well below that of the electrons [Pa84].

---

[1] The accuracy of the absolute value of the beam energy is, however, typically an order of magnitude worse than this (see Table 3.1), due primarily to the uncertainty in the ring circumference L_{ring}.

[2] Here, the lifetime is defined as $1/\tau \equiv (-1/N)dN/dt$, where N is the number of stored ions.

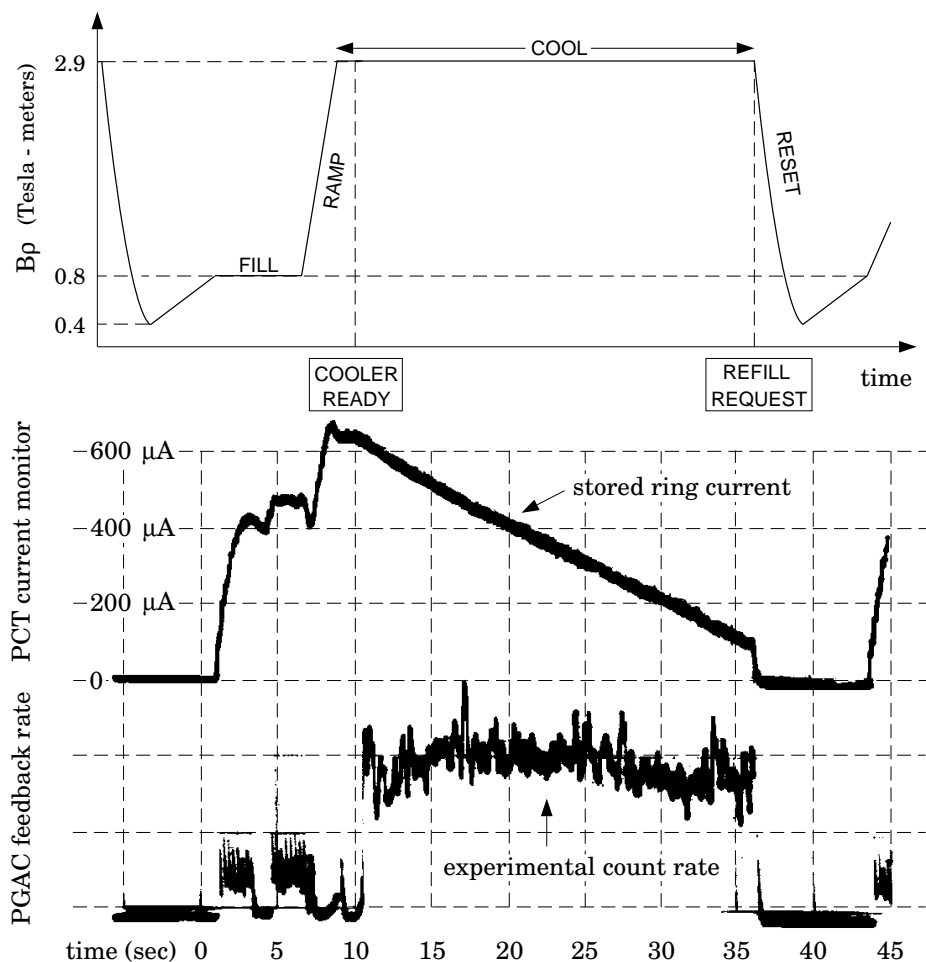Parameters characteristic of the cooling system at IUCF are shown in the lower half of Table 3.1.

Figure 3.3   A Cooler cycle typical to the CE-06 experiment. The upper half shows the time dependence of the ring rigidity for $E_p = 330$ MeV. The lower half displays the stored current and experimental data rate on the same time scale, taken from an actual scope display. The apparent increase in current during the ramp is artificial.

The operation of the Cooler is executed in cycles, since the experimental target depletes the beam and new particles must be injected periodically. Fig. 3.3 shows the time structure of a ring cycle characteristic to this work. The first part of the cycle is the beam injection from the main cyclotron into the ring. For an unpolarized proton beam, as needed for the CE-06 experiment, "stripping injection" is used. Using molecular hydrogen ions from the ion source, a 90 MeV H_2^+ beam is produced by the cyclotron, and stripped by a thin carbon foil in the I-region, resulting in a 45 MeV proton beam in the ring. Beam

is injected at the edge of the ring's transverse acceptance until the rate of particles gained equals the rate lost (usually after a few hundred msec).[3] The new beam is then moved away from the foil via bumper magnets and cooled so that the beam can be brought back again close to the foil for further injections. Typically, five to ten injection pulses are used per cycle. Cooling of the ions during the injection is critical to obtaining a highly intense stored beam: the circulating protons must be brought close to the (fixed) foil, which is located near the edge of the ring acceptance.

After injection is completed, often in a few seconds for unpolarized beam, a cool–ramp–cool sequence occurs. The cooling before acceleration increases the ramping efficiency by making the beam less susceptible to magnetic distortions or other effects which could normally bring some beam particles outside the ring acceptance. At the ramp top (defined by the ring dipole magnetic fields being constant), the beam is again cooled, at which time it is ready for experimental use.

The target is placed in the beam at this point, and cooling continues as particles are removed from the beam by the target. Given a total cycle time T, and a fill–ramp overhead time t_{oh}, the average luminosity over the cycle is

$$L_{\text{ave}} = \frac{N_0 f_{\text{B}} d_{\text{tgt}}}{T} \tau \left(1 - e^{-(T - t_{\text{oh}})/\tau}\right), \tag{3.1}$$

where f_{B} is the beam frequency, d_{tgt} is the average target thickness, and N_0 is the average number of particles injected per cycle. Here, the number of particles in the beam is assumed to decrease exponentially with a lifetime τ. The optimal cycle time T is found by maximizing this expression. The overhead time t_{oh} is usually fixed for a particular maximum current and beam energy, so that making T very small becomes inefficient, while making it too long may sample an excessive amount of the long, exponential decay tail. Similarly, increasing the target thickness too much may greatly reduce the lifetime τ, resulting in a lower L_{ave}, high background rates, or poor beam quality. For the CE-06 experiment, the cycle times ranged from roughly 30 to 45 seconds, with $t_{\text{oh}} \approx 15$ sec, and the beam lifetimes were directly controlled via motion of the target fiber, as detailed below.

3.2 Targets

The multi-pass nature of the recirculating ions in a cooled-beam storage ring often makes the choice of target crucial to the design of the experiment. Targets in storage

---

[3] The flux of protons leaving the ring is larger at this point than any at other time in the cycle; wire chambers that are sensitive to this background are operated at reduced bias during injection.

rings are typically much thinner than those in single-pass accelerator experiments, since a "thick" target ($d_{\text{tgt}} \approx 10$ μg/cm^2, for example) can heat the stored beam too rapidly for the cooling mechanism to compensate. Under these circumstances, the recirculated phase space volume may increase enough that all the advantages of cooling, including beam localization and good energy resolution, are lost. In addition, the high currents often available in storage rings (I $\approx$ 1 mA) would yield a very sharply peaked luminosity with such a target, resulting in high background and detector dead time problems. The cooling power of the ring effectively limits the internal target thickness to roughly 10^{16} atoms/cm^2, equivalent to about 200 ng/cm^2 of ^{12}C.

The heating of the beam via the target results in a finite lifetime of the stored current even when the target is thin enough that the cooling system can maintain a time-independent shape of the phase space distribution. This lifetime can have several components, the most important of which is usually transverse loss due to single and multiple Coulomb scattering of the beam with target nuclei. In this case, a particle scatters at an angle large enough to put it outside the ring acceptance, and it is lost.

For this process, the lifetime of the beam can be written

$$\frac{1}{\tau} \propto Z_{\text{tgt}}^2 \cdot f_{\text{B}} \cdot d_{\text{tgt}}^n, \tag{3.2}$$

where the dependence on the target's atomic number Z_{tgt} comes from the Rutherford cross-section. For a hypothetical zero-emittance beam, the exponent n is unity, but the value increases [Me85] to roughly 1.66 when the equilibrium non-zero emittances ϵ_x and ϵ_y are taken into account. In the latter case, "extra" particles are lost via $\epsilon_{x,y} \neq 0$ according to their proximity to the ring acceptance $A_{x,y}$. The probability of a beam particle leaving the ring after suffering a Coulomb scattering event can be characterized roughly by the ratios $\epsilon_{x,y}/A_{x,y}$.

Another beam loss mechanism occurs through the large changes in longitudinal momentum that can occur when a beam particle suffers a head-on collision with an atomic electron in the target. The beam particle is lost if the change in momentum is greater than the ring acceptance (see Table 3.1). More likely, however, the particle will remain inside the acceptance but will now experience only a very weak cooling force. Calculations have shown [Me85] that the equilibrium momentum distribution with a typical target and cooling force is very sharply peaked (see Fig. 3.4), with a long tail that contains these "slightly cooled" particles. The calculations further show that increasing the target thick-
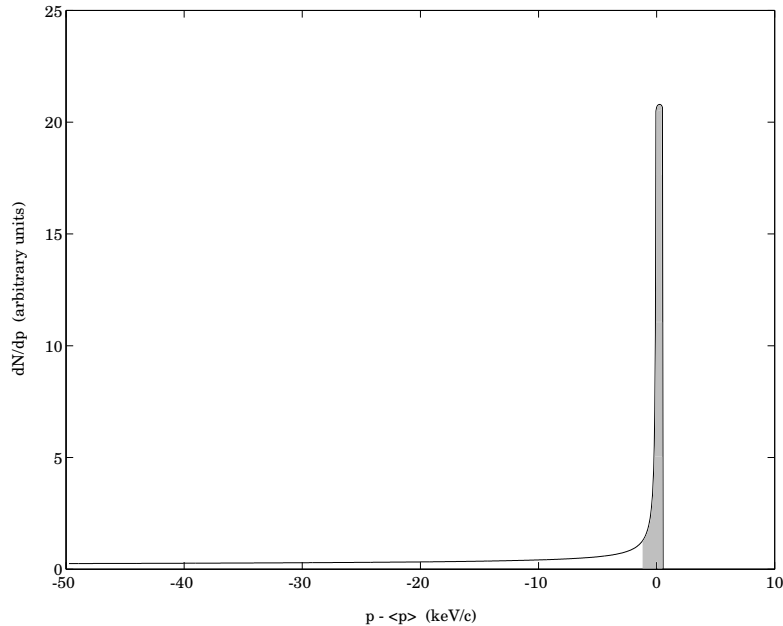
Figure 3.4   Relative momentum distribution of particles in a cooled beam, in equilibrium with a target. The calculation is for $E_{\text{beam}} = 200$ MeV with typical Cooler ring parameters. Beam particles within the shaded region (2 keV in width) primarily experience a cooling force $F_{\text{cool}} = -k(p - \langle p \rangle)$.

ness tends to raise the tail-to-peak ratio without a commensurate increase in the peak width.

Expression (3.2) shows that a thin target (for the Cooler, one with $d_{\text{tgt}} \approx 20$ ng/cm^2) can best take advantage of a cooled, stored, beam. In fact, a primary benefit of these targets for the CE-06 experiment is the dramatic reduction of energy losses of heavy recoils in the target material. Gas jet targets, which have been developed [Sp90] and used extensively at the Cooler, can attain thicknesses of 10^{13}–10^{15} atoms/cm^2 (0.2–20 ng/cm^2 ^{12}C equivalent) for several target species including Ar, H$_2$ and D$_2$. The targets work by forcing the gas through a thin (1–2 mm wide) low-temperature nozzle placed within millimeters of the beam. The gas target thickness is fairly well-controlled via adjustment of the flow rate and temperature of the gas jet nozzle.

The extent of the gas target is, however, large compared to a solid target. A typical gas distribution has 80% of the thickness within a few millimeters of the nozzle, with the remainder spread out over ten centimeters, so that an independent determination of the reaction vertex point must be made. Furthermore, in order to maintain the Cooler ring vacuum at the level of 10^{-8} torr, the pumping requirements are quite demanding: isolation of the target chamber from the ring via differential pumping stages is usually necessary.

The above considerations and the experimental target requirements for the CE-06 work led to the use of a solid target material. These requirements were primarily that:

a) The target should be thin enough to minimize $(\Delta E < 0.01 \cdot E)$ energy losses of recoil nuclei with $Z \geq 6$. With $dE/dx \approx 5$ keV/μg/cm^2 for particles with energies of 10–50 MeV, this implies a target thickness no larger than about 10 μg/cm^2.

b) The target should be localized in space enough that the reaction point is not a degree of freedom, and can be taken as "known." A point target is important for calculating the recoil rigidity from knowledge of its track through the magnetic field (see Sec. 3.3).

c) The atomic charge distributions of the recoil ions should attain equilibrium in the target material with preferential population of highly stripped states $(Q > Z - 3)$. Such stripping is necessary for the production of ions significantly less rigid than the beam so that magnetic separation is possible.

d) The target should be free of heavy contaminants such as ^{16}O.

Requirement (a) is met immediately by the Cooler target thickness restrictions which in fact are much more strict than this. A solid target is well-suited to (b) and allows transverse localization of the reaction point to the size of the beam (typically, less than 2 mm in diameter). The desired equilibrium charge distributions in (c) have been demonstrated in carbon targets down to 5 μg/cm^2 [Yu89] but are unknown for thin gas targets (in which an equilibrium may not be reached). Finally, though both gaseous (CH$_4$) and solid (graphite) ^{12}C targets are readily available with oxygen and other heavy contaminants at levels of better than one part in 10^6, isotopic purity (i.e., ^{13}C/^{12}C $\ll 1\%$) is generally harder (or impossible) to achieve in the case of methane compared to graphite.[4]

Given the choice of a non-gaseous target, however, one immediately notices that a self-supporting target cannot be used. A 5 μg/cm^2 target (roughly the limit to be self-supporting) has 2×10^{17} atoms/cm^2 and as such is too thick for the Cooler ring by at least an order of magnitude! New techniques were developed to present a time-averaged thickness to the beam which is significantly lower than the actual thickness.

One of these methods involves "wiggling" a thin carbon fiber across the beam, producing an effective thickness which is in the range needed for the Cooler (around 10 ng/cm^2). Typical dimensions of the fibers recently fabricated [Lz93] at IUCF are 3–10 μg/cm^2 thick

---

[4] The fiber targets used in CE-06 were, however, natural carbon (about 1% ^{13}C).

by 5 μm wide. These are made by carbon evaporation and condensation onto a finely polished glass substrate through a closely spaced wire grid. The "whiskers" are then floated off, annealed (to lower the intrinsic graphite resistivity), and attached to a frame with conductive glue.[5] The frame can then be wiggled mechanically with little stress placed on the fragile target.

For a fiber harmonically oscillating with amplitude x_0 across the beam (where x_0 is much larger than the beam diameter a), the average luminosity for a given sweep is

$$L_{\mathrm{ave}} = \mathrm{I}_{\mathrm{beam}} \cdot \frac{\xi}{\pi x_0}, \tag{3.3}$$

independent of the fiber frequency ν. Here, ξ is the linear density of the fiber, given by the product of the fiber's thickness and transverse dimension. From (3.3), the effective target thickness is just $\langle d_{\mathrm{tgt}} \rangle = \xi/(\pi x_0)$, so that for typical fibers and an oscillation amplitude of 1 cm, $\langle d_{\mathrm{tgt}} \rangle \approx 3$ ng/cm^2. Even so, since reasonably attainable fiber frequences for this amplitude are roughly 30 Hz, beam traversal times for the whisker are on the order of one msec. Hence, the target moves very slowly as seen by the beam, which makes about 1000 revolutions in this time. This contradicts the prediction of Eq. (3.3) that the target thickness is characterized by $\langle d_{\mathrm{tgt}} \rangle$ rather than d_{tgt}, the latter being much too thick!

Experiment and simulations [Pz93] have shown, however, that Eq. (3.3) is indeed correct: the lifetime and energy spread of the stored beam are essentially the same as that for a homogeneous gas target with the equivalent thickness $\langle d_{\mathrm{tgt}} \rangle$. The inhomogeneous nature of the fiber target over the extent of the beam allows a particle which has been heated by a target collision to have a negligible interaction probability over the next few msec and thus become cooled again. The lifetimes predicted by simulation agreed with experiment after it was realized that the fiber was charging up and electrostatically deflecting a fair amount of the beam current; conductive glue was used to prevent this effect.

There are, unfortunately, several experimental disadvantages associated with the wiggling fiber target. One of these stems from the fact that the low average thickness depends on the fiber being outside of the beam for 90% of the total "target in" time. The average luminosity in (3.3) consists of 1 msec-long "spikes" in the luminosity, each of which is characterized by a central value $L_{\mathrm{max}} \propto N \cdot f_{\mathrm{B}} \cdot \xi$, where N is the number of particles in the beam at the time of the sweep. These peaks are separated by 10–15 msec intervals of

---

[5] The conductivity of the glue turns out to be important to prevent the fiber from charging up.

zero luminosity. The ratio $L_{\text{ave}}/L_{\text{max}}$ is, in this case, just the amount of time spent in the beam:

$$\frac{L_{\text{ave}}}{L_{\text{max}}} \approx \frac{a}{2x_0}. \tag{3.4}$$

This "duty factor" for a typical fiber oscillation is $2\,\text{mm}/2\,\text{cm} = 0.1$. Given a (roughly) fixed number of particles N_0 available per cycle, it is best to maximize the duty factor (3.4) so as to minimize the accidental coincidence rate.[6] Note that for a particular target thickness, the maximization of Eq. (3.1) is equivalent to maximizing the duty factor.

Another difficulty involved with the use of the oscillating target is related to the standard IUCF readout/data acquisition system, which requires a dead time period of approximately 1 msec between event triggers. Since each fiber pass through the beam consumes the same amount of time or less, only one trigger is possible per sweep, and two per oscillation period. Assuming that the counts per sweep are distributed according to Poisson statistics, the experimental live time is

$$\varepsilon = \frac{\text{triggered events}}{\text{all events}} = \frac{2\nu}{n}(1 - e^{-n/2\nu}), \tag{3.5}$$

where ν is the fiber frequency and n is the average number of triggers per unit time: $n \propto L \cdot \sigma_{\text{t}}$. Here, σ_{t} is the total effective cross-section for any reaction events capable of producing event triggers. Even for $n = 2\nu$, i.e., one trigger on the average per fiber sweep, $\varepsilon = 0.63$ and decreases rapidly as n increases.

Consequently, the experimental efficiency is quite low unless either the fiber frequency can be greatly increased (for example, to 1000 Hz) or n can be reduced via fast hardware rejection of background events (included in σ_{t}). For fiber amplitudes in the range of several millimeters, the only means to achieve such high frequencies may be through oscillating the beam rather than the target. This capability has not yet been fully developed at the T-site of the Cooler ring.

The second tested means of using thick targets in the Cooler, and the method used for this work, involves "skimming" the beam with the target. Here, an open-edged foil or fiber (both with $d_{\text{tgt}} \approx 5$ $\mu\text{g}/\text{cm}^2$) are moved slowly into the beam from the edge, skimming off beam particles that are already in the tails of the beam's transverse phase space. This technique is essentially equivalent to decreasing the ring's transverse acceptance slowly in time. In this way, the cooled properties of the rest of the beam are essentially left

---

[6] For the CE-06 experiment, this rate was just $R \propto R_{\text{pgac}} \cdot R_{\text{pc}} \propto L^2$. See Sec. 3.4.

unaffected. No true heating-cooling equilibrium is obtained in this way, however; essentially any particle interacting with the skimmer target is lost via one of the mechanisms described above. If the experimental data rate can be controlled, the duty factor of the skimmed target can be much better than that for the wiggled fiber.

The lower half of Fig. 3.3 shows the beam current and experimental count rate for a typical skimmed-target cycle of the CE-06 experiment. Two graphite fibers of thickness 4.2 μg/cm^2 and widths of 3.3 μm and 8.3 μm were mounted on a target ladder along with a 6.2 μg/cm^2 foil.[7] The horizontal ladder was attached to a rod which could be moved perpendicularly to the beam using externally controlled stepper motors. The external control device [Pp90] was an IBM PC running software allowing specification of all the target motion parameters (e.g., start point, stop point, velocity) and readout of the absolute position of the ladder. The rate from one of the CE-06 detectors (namely, the PGAC, see Sec. 3.4.2) was used as a negative feedback input: if the count rate was too low or high compared to a software rate parameter, the fiber was moved toward or away from the beam center, respectively. The position of the targets with respect to the beam center were measured for each new ring tune, to account for the small transverse shifts in the beam (on the order of 1 mm) from one energy to another.

A successful cycle (as shown in Fig. 3.3) occurred when the experimental count rate was essentially flat over the beam lifetime. The time-averaged luminosity, and the duty factor, was maximized in this case by increasing the control PC's rate goal parameter, while maintaining a reasonable data acquisition live time (at least 80%). In this way, the beam lifetime is decreased, allowing a shorter total cycle time and therefore a larger number of particles used up per unit time.

The primary concerns about this mode of target operation mainly involve background rates, due to the use of a thick target presented at the phase space edge. Most of this background consists of particles scattered at small angles in the target which leave the ring due to their proximity to the surface of the phase space volume. Initial tests of the CE-06 apparatus at the T-site showed that this background did not present any problems for the experiment, especially when the rate feedback mechanism was employed.

3.3   The T-Site Magnet

The centerpiece of the T-region of the Cooler ring is a large-gap dipole magnet, capable

---

[7]   The foil was held with one edge open in a "C" frame.

of bending the beam by six degrees (see Figure 3.5). The beam is bent by the magnet into a small exit pipe, allowing either the detection of 0° neutral reaction products or, as in the CE-06 experiment, the magnetic analysis of soft reaction products emitted at small angles to the beam.
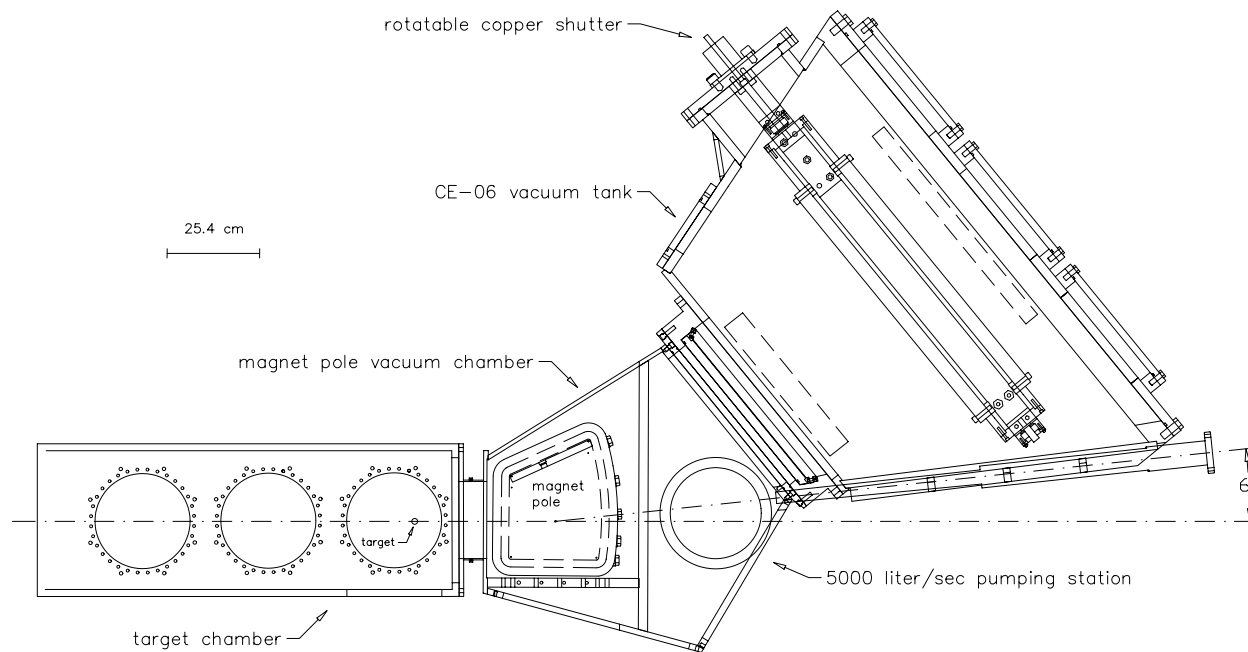

Figure 3.5   Schematic of the accelerator and vacuum apparatus *in situ* at the T-site. The beam circulates from left to right in the figure. Shown for comparison are the locations of the CE-06 detector housings (dashed boxes) and target position.

In order to provide the capability of high solid angle efficiency for proximate detection systems, the physical design of the 6° magnet (shown in Figure 3.6) is quite different from the other ring dipoles. The most experimentally important feature of the magnet for this work is the large vertical gap of 12.7 cm, which allows the passage of emission projectiles with vertical angles between $-6°$ and $+6°$. The geometric horizontal aperture of the magnet, for positively-charged reaction products, extends roughly between $+8°$ and $+20°$ toward the inside of the ring.

These geometrical parameters are particularly important in experiments such as this work where the reaction projectiles of interest are emitted at small angles with respect to the beam and high acceptance efficiencies are needed. For ^{12}C$(p, \pi^+)^{13}$C, at $E_p = 166$ MeV, for example, the recoil ^{13}C ions are emitted in a narrow forward cone of half-angle 3.4°, all of which are accepted through the magnet gap. Use of the more conventional ring
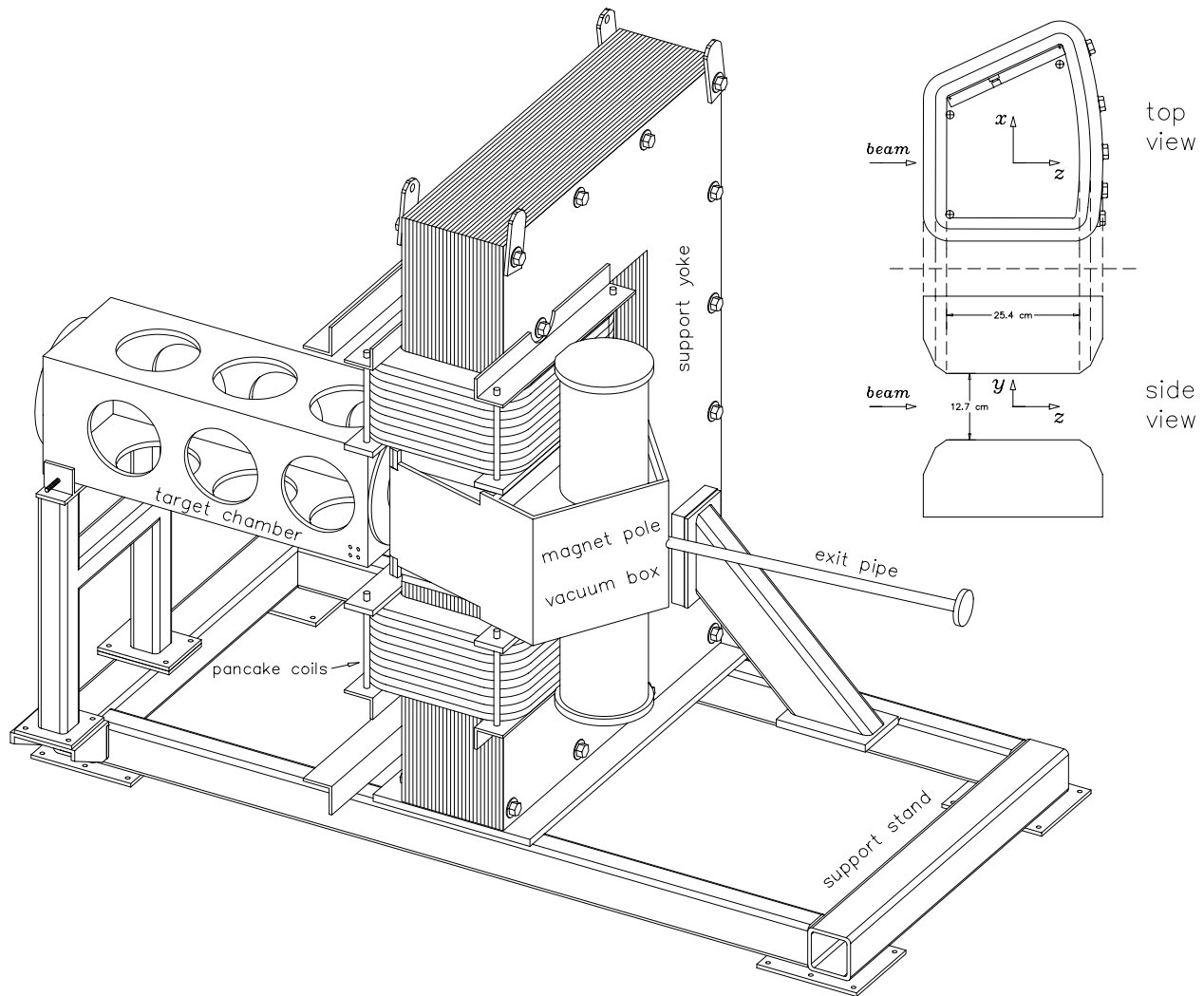
Figure 3.6   The 6° dipole magnet design: entrance box (the large number of ports necessary for pumping support of gas jet targets), support structure, and exit pipe (at 6° with respect to the entrance). Also shown are the top and side views of the magnet poles, along with the magnet coordinate system defined in App. C.

dipoles with typical available gaps of about 5 cm would reduce the geometrical acceptance by at least a factor of three. The large solid angle afforded[8] by the 6° magnet can be especially critical for near-threshold studies of other reactions where the cross-sections are small ($L\sigma \ll 1$ sec^{-1}).

The multi-ton yoke of the magnet serves to contain the field, support the weight of the coils (about 150,000 amp-turns), and resist the attraction of the pole faces (about one ton of force). Figure 3.7 shows the current in the coils needed for a given proton momentum.

---

[8]   This is indeed the single most expensive design parameter, via the vertical gap, of the T-site magnet.

The magnet was built to be operated well below saturation, even at the maximum design strength of 3.76 Telsa-meters. To enhance further the fast ramping ability needed for Cooler operation (see Table 3.1) and to minimize eddy currents, the pole faces were fabricated from laminated iron slices 1.25 cm thick.
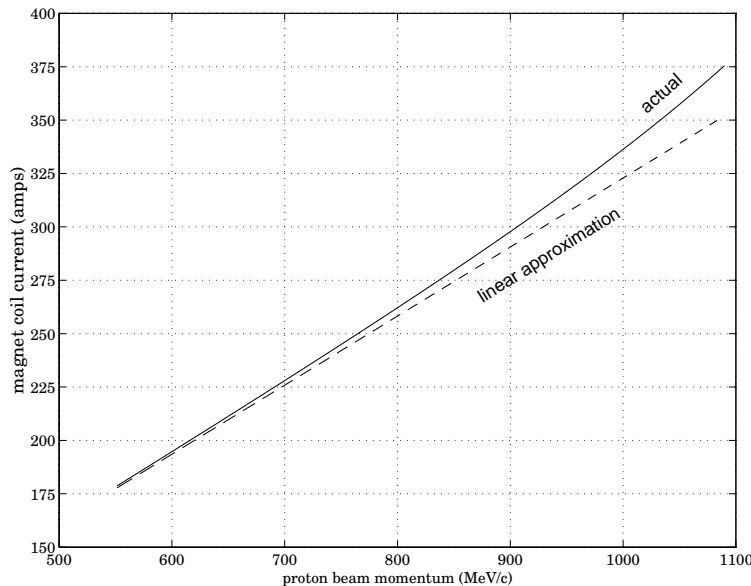

Figure 3.7   Current vs. beam momentum for the six-degree magnet. Shown
for comparison is the linear approximation I $\propto$ p, matched for $p \to 0$ to the
actual relationship. The true current at the top of the Cooler ramp may vary
from that shown by 1–2% according to the particular beam tune.

Standard magnet-mapping techniques were used at IUCF to measure the y-component[9] of the field in the x-z plane ($y = 0$) and at several out-of-plane y values. Calculations were then performed (see App. C for details) to construct a uniformly-spaced three-dimensional grid of **B** from this data. Characteristic plots of the magnetic field for I = 300 amps ($E_p \approx 365$ MeV) are shown in Fig. 3.8. The dimensions of the "flat" part of the field ($B > 0.9 \cdot B_{\mathrm{max}}$) are approximately 24 × 24 × 8 cm and the field is large ($B \gtrsim 0.1 \cdot B_{\mathrm{max}}$) and non-uniform over a considerable extent. Particles that deviate by more than a few degrees from the 0° median-plane path heavily sample the B_x and B_z components of Fig. 3.8. The fully three-dimensional raytracing calculations (described in App. C) are therefore necessary for magnetic analysis of charged reaction products via the CE-06 detector stack.

---

[9]   The coordinate system used in this work (referred to as "magnet" coordinates) is defined in Fig. 3.6
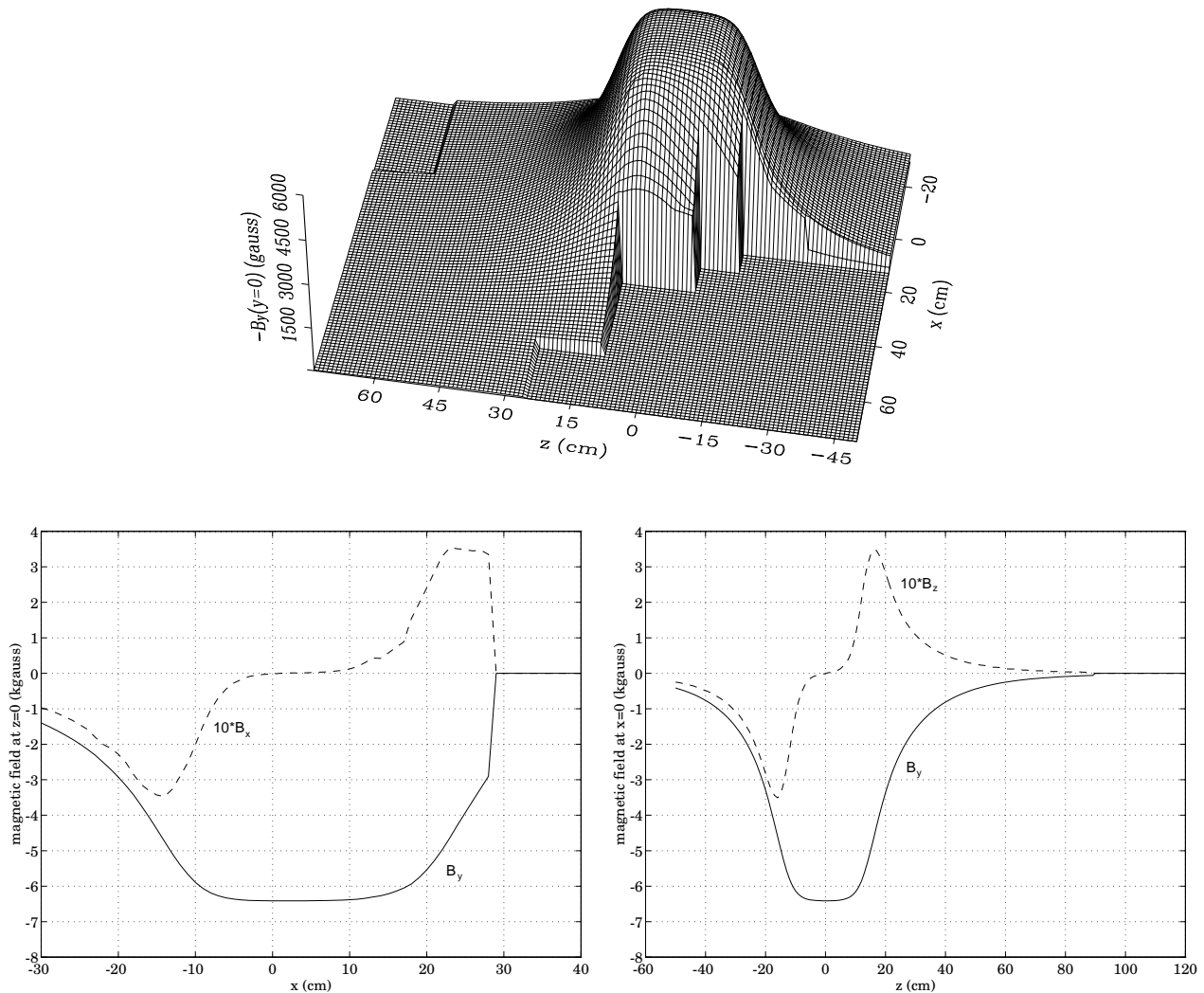and App. C.

Figure 3.8   The 6° magnet dipole field for I = 300 amps. At this current, $B_{\mathrm{max}} \equiv B_y(0,0,0) \approx 0.6$ Tesla. The median plane ($y = 0$ cm) values of B_y are shown; the plots for B_x and B_z correspond to $y = 1$ cm.

3.4   The Detector Stack

3.4.1   Overall Setup

The detector apparatus used for the CE-06 experiment was primarily designed to detect medium-weight recoils with $Z = 3$–8 in the energy range of 1.5–4.5 MeV/amu with extremely high efficiency. A fundamental concern for a detection system of this type is the reduction of unrecoverable ion energy loss, e.g., losses in pressure foils or in gaseous dead layers. To avoid ion energy losses in air, the CE-06 detector stack was enclosed in a vacuum box attached directly to the exit flange of the 6° magnet box. The complete vacuum enclosure was needed since recoils in the middle of the energy range (3 MeV/amu, $Z = 5$)

experience energy loss at the rate of about 2 MeV per mg/cm^2 of material traversed.[10] Figure 3.9 shows the vacuum box along with the CE-06 detectors in their run positions. A large-area (roughly 1000 cm^2) valve attached between the box and the magnet chamber afforded independent pumping operation or detachment of the CE-06 tank. A thin pressure foil (1 μm of Mylar) covered the flange opening to provide for isolation of the 10^{-8} torr ring vacuum from the 10^{-6} torr tank pressure.
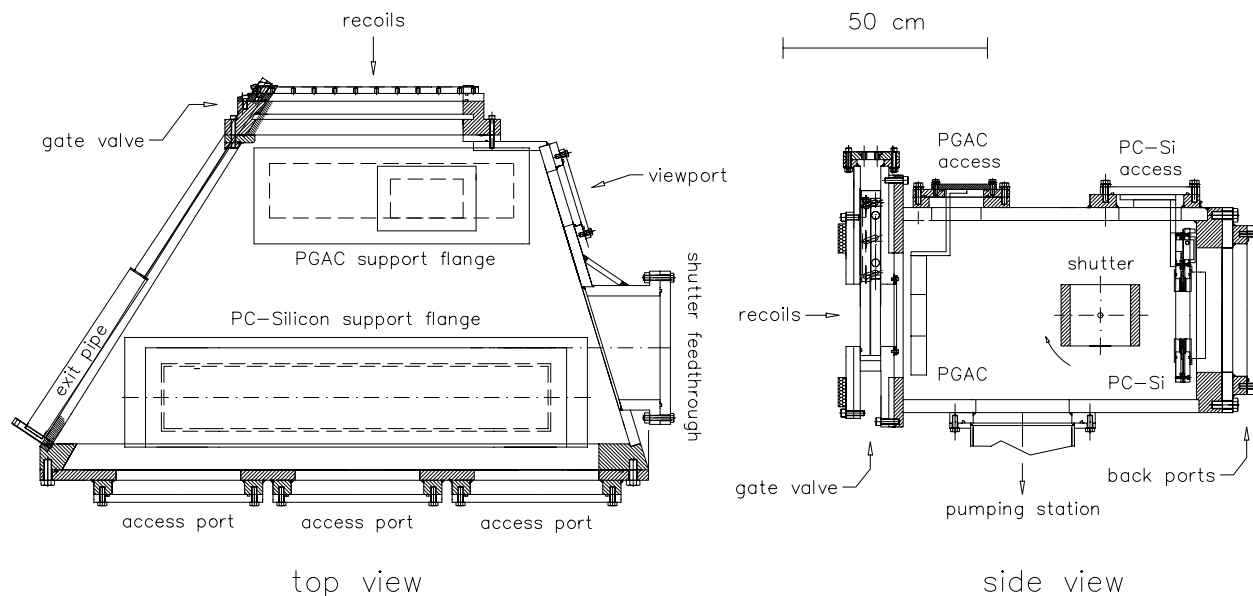
Figure 3.9   Top and side views of the vacuum tank attached to the T-site magnet for the CE-06 experiment. Not shown are the support platform and casters on which the box was mounted to allow it to be rolled back from the attachment flange. The shutter is shown in closed position.

The CE-06 tank provided ports on the top, through which the detectors were mounted into the tank, and whose flanges doubled as support mounts for the detectors. More ports were built into the back (used for cable feedthroughs) and the bottom (for a low-impedance pumping port). Also housed in the tank was a slow-acting "shutter", externally rotatable via a ferrofluidic feedthrough, and consisting of two copper slabs totaling 90 g/cm^2 in thickness. The shutter provided complete protection for the silicon detectors (see Sec. 3.4.4) against 45 MeV injection protons and partial blockage of protons of up to 300 MeV, at times when the experiment was not on-line at the Cooler. Although external motor control coupled to the ring cycle would have made on-line injection background protection possible,

[10]   A thickness of 1 mg/cm^2 is equivalent to 4 μm of Al, 7 μm of Mylar, or 8.6 mm of air at STP.

proton count rates on the silicon array were small enough under CE-06 running conditions that this protection was not necessary.

For the reactions of interest in this work, recoil ions with masses comparable to the ^{12}C target nuclei are emitted with roughly the same momentum as the circulating proton beam. The ions are typically highly stripped for the energies of a few MeV per amu and so are bent by $Q \cdot 6°$, where $Q \geq 2$, allowing complete separation of the ions from the beam. Figure 3.10 shows the known charge distributions [Ba81] for the recoils of interest; carbon and nitrogen recoils are typically emitted with $Z - 3 \leq Q \leq Z$.
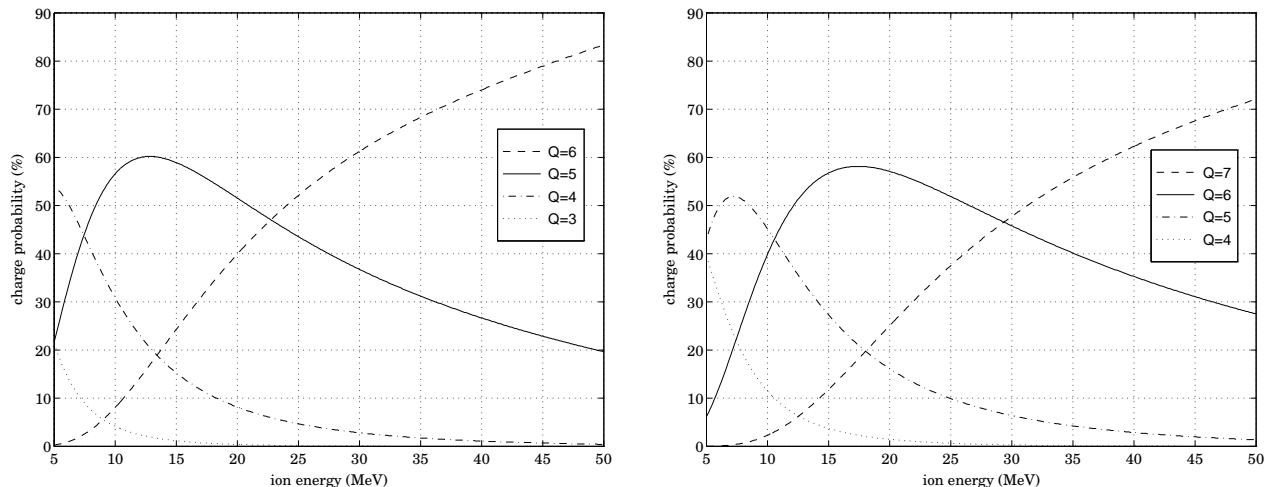
Figure 3.10 Carbon (left) and nitrogen (right) atomic charge distributions. Shown is the probability that an ion with energy E will have charge Q after passage through carbon foils. Other works (e.g., [Yu89] and [Bn68]) have verified the population of highly stripped ions for foils as thin as those used in CE-06.

These distributions are the result of reaction emission ions attaining an equilibrium charge by "pickup" of atomic electrons during passage through the target material. Highly energetic recoils are therefore less likely to experience recombination and tend to remain fully stripped. "Re-shuffling" of the atomic charge can occur whenever the ion passes through matter; however, raytracing (see App. C) showed that, even at the location of the pressure foil, the magnetic field was too weak for this charge change to have a noticeable effect on the direction of the ion track.[11]

A schematic of the detector setup for CE-06 in position at the Cooler T-site is shown in Fig. 3.11, along with calculated median plane projections of flight paths for several important ion species (using single-pion production kinematics at $E_p = 350$ MeV). The

---

[11] At least, when compared to the effect of multiple scattering, see Chapter 4.
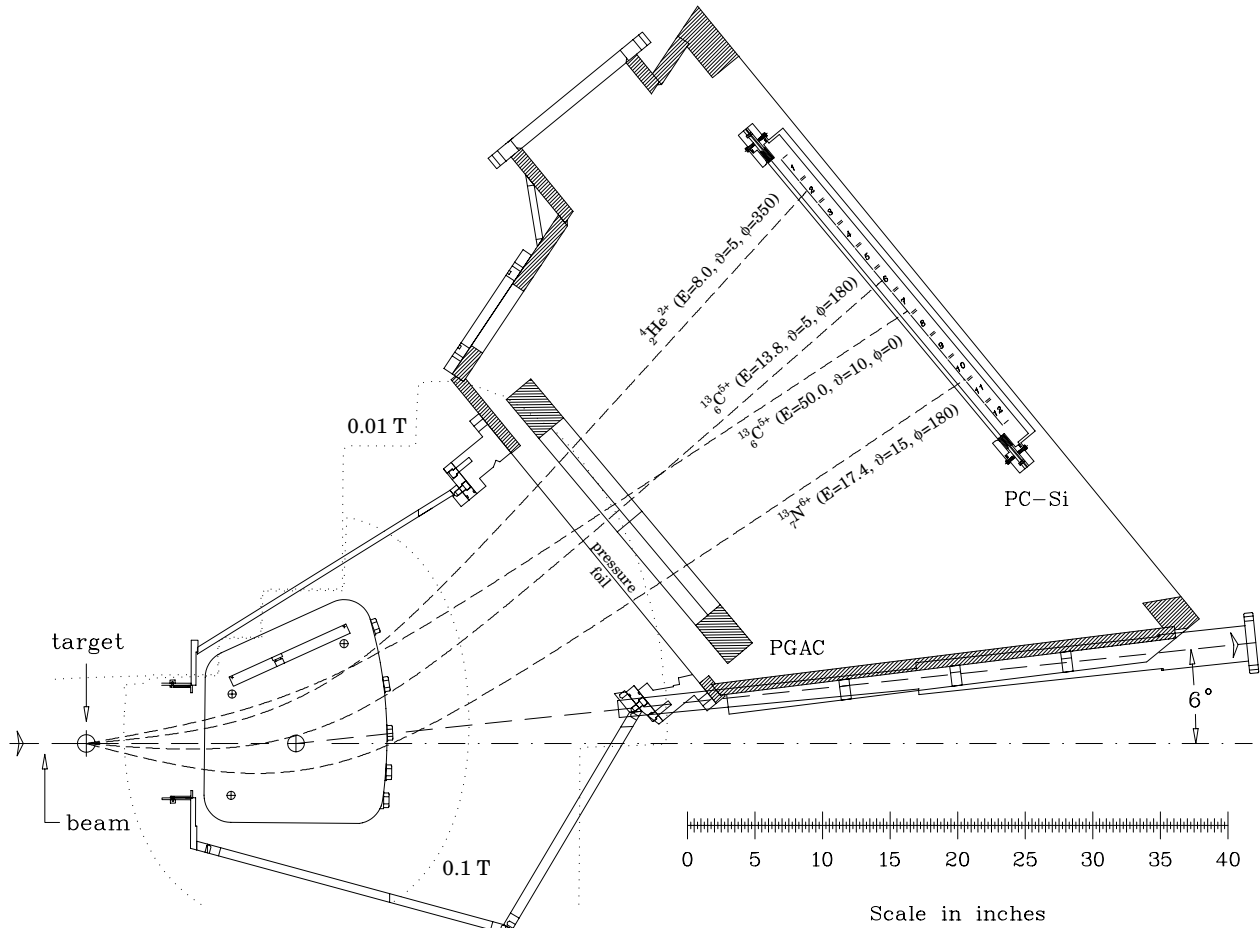
Figure 3.11 The detector apparatus for CE-06 at the T-site, shown with the 100 and 1000 gauss boundaries of B_y for $E_p = 350$ MeV. The target was approximately 38 cm from the field center ⊕. Ion tracks, specified by reaction energies (MeV) and angles (deg), are shown projected into the plane $y = 0$.

figure also shows that $^4_2\text{He}^{2+}$ ions with energies characteristic of common laboratory sources (several MeV) have the proper rigidity to be transported through the detector stack. This fact was used to advantage in CE-06 as a means of position, energy, and timing calibration of the entire detector stack *in situ* off- and on-line.

With the knowledge of the detector locations and the magnetic field, coupled with the absolute calibration of the raw energy and position signals in particular, the CE-06 detector stack provides the complete identification of recoils along with the determination of the reaction angle θ at the target. The PGAC and Si detectors measure the velocity vector of an ion (all components) by determining its position and time-of-flight. The transmission proportional counter (PC) measures the ion energy loss dE/dx which, coupled with the energy measurement made by the Si array, identifies the ion atomic number. The

knowledge of **B** and the target location completes the picture by determining Q, M, and the reaction angle θ. Since the PGAC and PC are "low-pressure" detectors (cf. App. A), this can be accomplished efficiently for $Z > 3$ with relatively little sensitivity to protons and α particles. A full discussion of the calibration and data analysis for the CE-06 experiment is found in Chapter 4. The remainder of this chapter describes the detector hardware in detail.

3.4.2 The Parallel Grid Avalanche Counter

The Parallel Grid Avalanche Counter, or PGAC, is a low-pressure transmission detector designed to provide two-dimensional position information along with fast timing of highly ionizing particles (see App. A for a more complete discussion of general and low-pressure gas detector operation). The PGAC used in the CE-06 experiment was constructed with grids rather than foils (which would produce a PPAC, where the P stands for "Plate" [Rm88]). In this way, only two foils[12] were necessary (as pressure foils), so that the total detector thickness was kept below roughly 250 $\mu g/cm^2$.

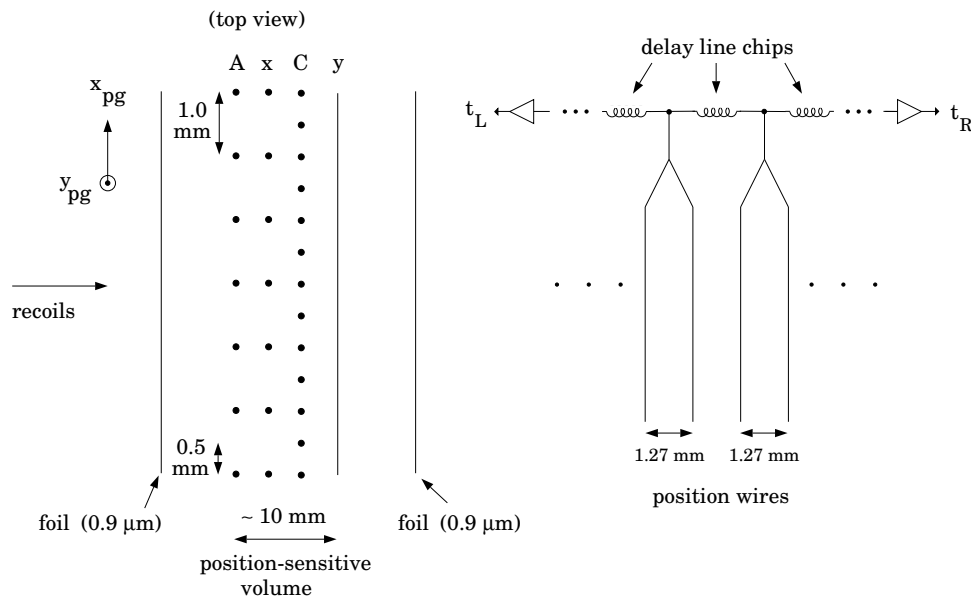*Figure 3.12*   Schematic view of the PGAC active volume, with relevant dimensions. All grids are 20 μm Au-plated tungsten except for the cathode (10 μm). Also shown is the equivalent circuit for the internal delay line. Each delay element separates two position wires.

The PGAC is comprised essentially of four wire grids, shown schematically in Fig. 3.12,

---

[12] All of the foils used in the CE-06 experiment (including the isolation pressure foil) were 0.9 μm thick non-aluminized DuPont Mylar.

which allow a total transmission efficiency of 95%. The two main electrode grids, the cathode (C) and the anode (A), are biased to roughly -310 V and $+300$ V, respectively. PGAC operation for CE-06 involved bias voltages of up to ±320 V but this was often limited by sparking caused by the relatively large proton background flux during ring injection. With a standard operating gas pressure of 3 torr of isobutane, the PGAC runs in avalanche mode: the 600 volts of potential across the 6 mm gap between the anode and cathode is no further than roughly 10% from the sparking threshold. The negative signal induced on the anode is therefore saturated and fast (typical risetimes are 2–3 nsec). The intrinsic timing resolution of the PGAC using this signal was measured and found to be roughly 400 psec.

The PGAC can also detect the position of an incident ion as it passes through the active volume. Position determination is accomplished by placing electrode grids close to the avalanche grids (C) and (A) in such a way as to minimally disturb the avalanche field configuration. In this case, the x-position grid (measuring displacement along the detector length) is held at ground and located halfway between the cathode and anode. The y-position grid (for displacement out of the plane of Fig. 3.11) is also grounded and is placed behind the anode by half the cathode-anode spacing.

Signals are induced on the position grids in the same way that a pulse is formed on the cathode of a cylindrical proportional counter. As such, they are positive-going and quite small compared to the anode signal. One of the benefits of the avalanche mode of operation is the large multiplication factor, which causes relatively large induced signals on the positions grids. For the PGAC position grid wire spacing of 1.27 mm, an induced signal appears on several wires, even at normal ion incidence, due to the large electron mean free path at these gas pressures.

In order to reduce the amount of electronics that would be necessary to readout all 450 position grid wires in the PGAC, the ends of the wires are connected to a passive delay line, as in Fig. 3.12. The PGAC is separated electrically into two halves along the x-direction so as to minimize attenuation of the induced signal in the delay line.[13] The signals at each end are fed into a TDC's stop inputs with the anode signal for a start. If x_{pg} is the position of an ion path from one end of the delay (total length L) and Δt is the incremental delay between position wires, then

$$t_{\mathrm{left}} = (\Delta t)x$$

---

[13] The bifurcation also improved the detector's event rate capability.

and

$$t_{\text{right}} = (\Delta t)(L - x)$$

so that

$$t_{\text{left}} - t_{\text{right}} = (2\Delta t)x + \text{C}. \tag{3.6}$$

Here, C is a constant depending on the total PGAC delay line length, differences in lengths of the coaxial cable leads, and on offsets in the TDC. The subtraction of the two TDC channels is therefore proportional to the ion position x_{pg} (the method used to determine the ion vertical position y_{pg} is, of course, completely equivalent).

The purely inductive nature of the position signal (there is no actual charge avalanche or multiplication at these wires) implies a non-linear fall-off in its amplitude with distance from the center of the ionization track: $V_{\text{ind}} \propto d^{-n}$, with $n > 1$. Therefore, although the effective wire spacing for the position grids is 2.54 mm, resolutions significantly better than this can be attained. Tests of the PGAC in a spectrograph with an α source showed the position resolutions (scaled to normal incidence ion tracks) to be 1.3 mm and 1.8 mm for x and y, respectively. In general, the resolutions improve for more highly ionizing particles and larger cathode-anode differential voltages, both of which increase the size and risetime of the induced position signals.
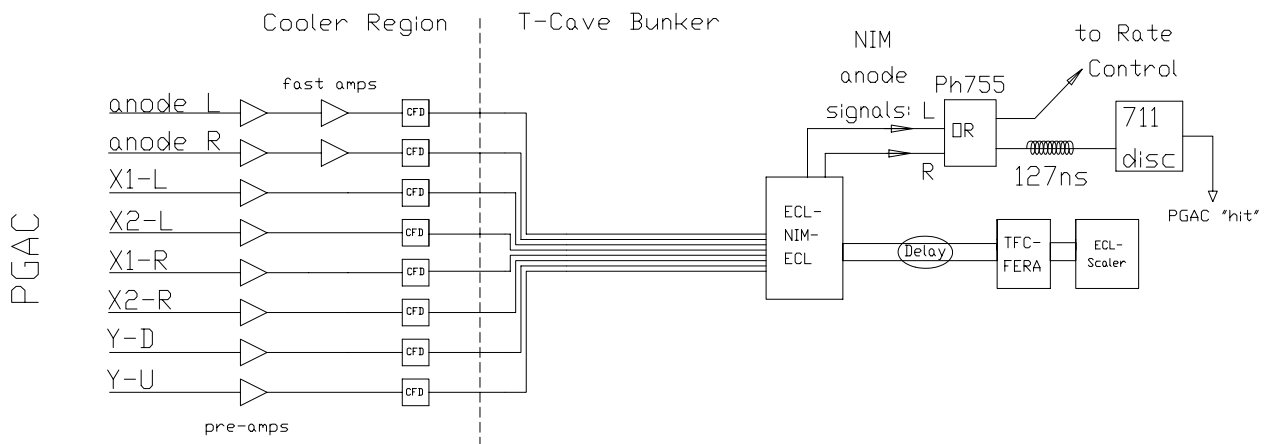

Figure 3.13   The PGAC electronics. All components shown to the left of the dashed line were mounted directly on top of the CE-06 vacuum tank, and connected via vacuum feedthroughs in the PGAC support flange shown in Fig. 3.9. Further details of the T-Cave electronics are given in Sec. 3.5.

The readout electronics used in CE-06 for the PGAC were quite simple due to the delay-line configuration (see Fig. 3.13). The split anode and x-position grid results in two

anode signals and four x-position signals, along with a small dead area between the two anode grids of roughly 3 mm. The near-normal incidence of recoils in the CE-06 experiment (see Fig. 3.11) typically implies a one-to-one correspondence between anode and x-position grid halves.

3.4.3   The Proportional Counter

The Proportional Counter, or PC, was the next major component of the CE-06 detector stack, proceeding outward from the magnet. Like the PGAC, the counter is a low-pressure detector, but it is designed to be operated at high-enough pressures ($P \gtrsim 10$ torr) to be in the proportional mode. In this mode, the PC measures $(\Delta E / \Delta x)_{\text{ion}}$, the ion's energy loss per unit thickness of the detector's active volume. Coupled with a measurement of the ion velocity v, the counter determines Z_{ion} from

$$\frac{\Delta E}{\Delta x} \propto f(v) \cdot Z^2, \tag{3.7}$$

where f is a known function. If the ion's incident energy E is known, the mass M and nuclear charge Z are measured via

$$\Delta E \cdot E \propto M \cdot Z^2. \tag{3.8}$$

In principle, it is also possible to measure the ion's atomic charge Q via[14] the transmission energy loss; however, the variation in deposited energy is less than 1% for nitrogen ions with $E \gtrsim 10$ MeV.

There were three main design goals for the PC as developed for the CE-06 experiment. One of these was the maximization of the solid angle subtended to the target. Given reasonable dimensions of the vacuum enclosure on one hand and the benefits of a long time-of-flight (TOF) path on the other (see Fig. 3.11), the active area of the PC needed to be about 10 cm vertically by 65 cm horizontally. With a TOF path length of roughly 60 cm, this would result in a geometrical solid angle of $\Delta\Omega \approx 20$ msr.

Another desired feature of the PC was the ability to measure $\Delta E / \Delta x$ for a wide range of ion types and energies. In particular, good resolution (requiring a thicker active volume) and transmission capability (requiring the reverse) was needed for ions with $5 \le Z \le 8$ and 10 MeV $\lesssim E_{\text{ion}} \lesssim 50$ MeV. For the operating gas CF_4 (carbon tetrafluoride), calculations using standard energy loss tables for elements [No70], along with interpolations

---

[14]   The specific energy loss of the ion decreases as it captures electrons from gas or foil molecules.

to compounds [Ce75], suggested that a 1 cm thick active volume with pressures in the range of 20–100 torr would be optimal.

The final important capability of the PC was position sensitivity in the y-direction (out of the page in Fig. 3.11). Together with the PGAC y measurement, this information would provide a complete determination of the vertical direction cosine of the reaction ion. At the desired position for the PC, the resolution needed to achieve a vertical angular resolution of 0.1° is $\Delta y \lesssim 5$ mm.

To test the feasibility of attaining these goals, a prototype detector was constructed, using the sense plane parameters (e.g, anode wire spacing) expected for the full-scale device, but with a 5×5 cm active area. Top and side views of the active region are shown in Fig. 3.14. As in the PGAC, wire grids were used as cathode planes instead of foils to minimize energy losses.
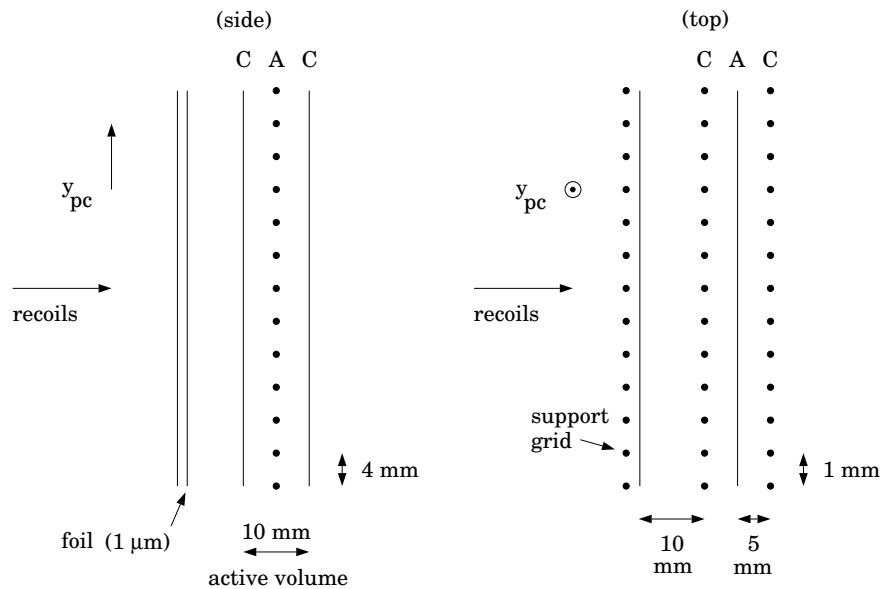
Figure 3.14   Schematic (not to scale) of the operational design of the PC. The prototype detector consisted of only the anode (A) and cathode (C) grids (supported on a small G-10 frame) and was operated in a separate gas enclosure.

To allow the capability of the measurement of y, the PC is actually an MWPC (multi-wire proportional counter): the anode plane consists of electrically independent wires spaced by 4 mm (the prototype wires, however, were OR'd together due to lack of space for separate readout). Assuming that only one wire fires per ion event, the vertical resolution of the PC is simply $\Delta y = 4$ mm. The single-wire behavior in MWPC's was in fact confirmed [Ch68] many years ago; however, whether the PC wires would each act as an

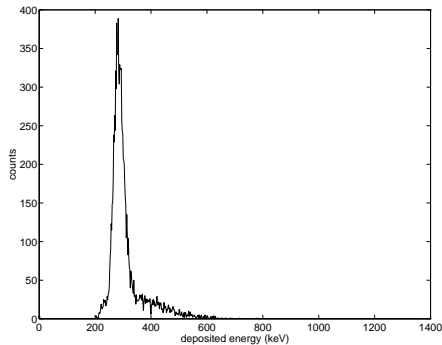independent detector or not, given the heavy ionization tracks that would occur in CE-06, was not known.

Figure 3.15

The prototype was initially tested with an α source, using a single charge-sensitive pre-amp for the combined anode wires, at a variety of gas pressures and anode biases to check stability and resolution. The figure at left shows the PC energy spectrum obtained at a typical operation point: 100 torr of propane (similar to CF_4 but with less stopping-power) and $V_{bias} = +1000$ volts. The achieved resolution was approximately 5% FWHM, which was better than expected given the relatively small energy loss of the α particles in the active volume (about 200 keV).

To determine the counter performance for more highly ionizing particles, tests with the prototype were carried out at the Princeton University Cyclotron. A 5×5 cm silicon detector[15] was placed directly behind the back cathode grid of the prototype, also immersed in the gas. The main goal of the prototype test was to determine the quality of particle identification possible by measuring ΔE and E.

A 48 MeV α-particle beam from the cyclotron was bombarded on a ^{12}C target to produce a variety of ion species at energies appropriate to CE-06 (up to about 25 MeV). The results of the test, shown in Fig. 3.16, were good: a clear Z separation of the ions was achieved for $Z = 4$, 5, and 6 ($Z = 2$ and $Z = 3$ were also well-separated but off the scale in the figure). The first excited state of ^{12}C at 4.4 MeV is clearly visible in the $Z = 6$ group in the region of silicon energies around 19 MeV, along with the 15.11 MeV state near $E_{si} = 7$ MeV. The ^{12}C ground state (populated weakly at this level of momentum transfer) can also be seen close to $E_{si} = 23$ MeV.

At this stage, the full-scale PC was designed and built. Front and side views of the completed counter are shown in Fig. 3.17. Several important features of the final detector as built do not exist in the prototype. One of these is the support grid for the pressure foil. Tests with the thin (1.0 μm thick and 650 cm^2 in area) Mylar foil showed that it would not hold more than about 10 torr while supported only at the edges. Consisting of

---

[15] The Si detector was itself a prototype of the CE-06 detection system; see Sec. 3.4.4.
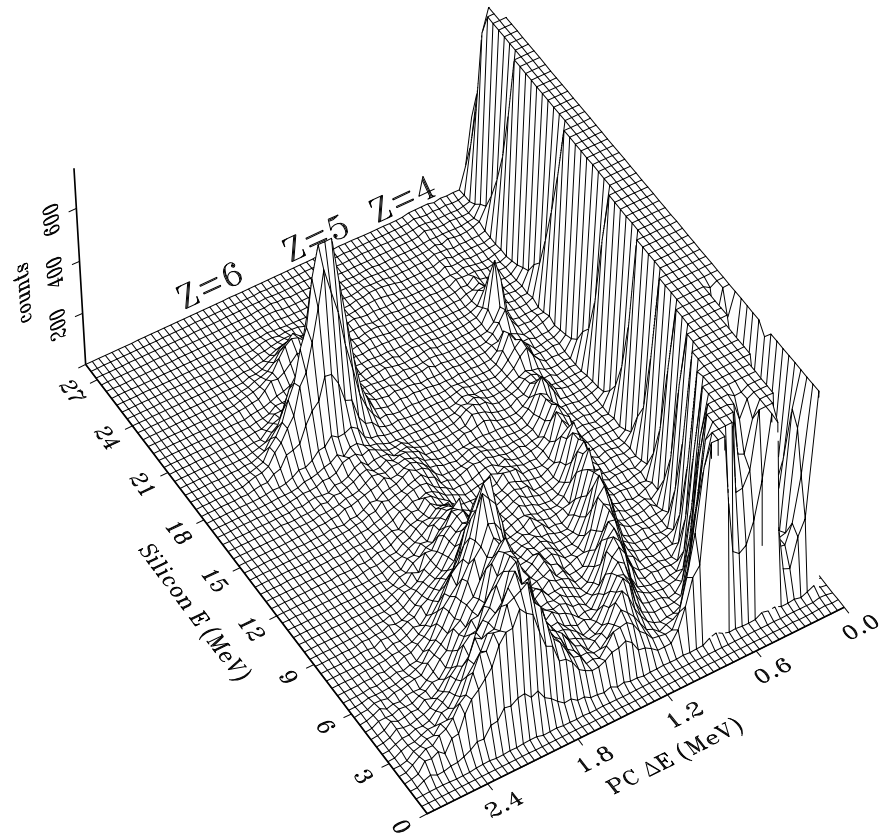
Figure 3.16   Particle identification using the prototype counter and silicon detector, both with active areas of 5×5 cm. The prototype ΔE calibration shown is reliable only for the $Z = 6$ ions.
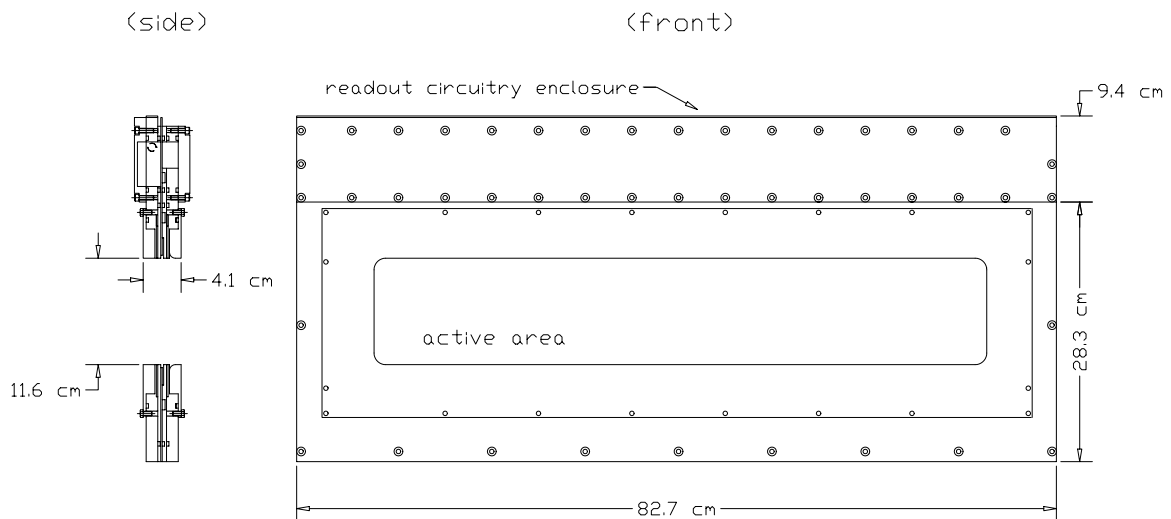

Figure 3.17   The CE-06 Proportional Counter. The pre-amp chips and associated electronics for each wire are contained in the small chamber at the top of the PC proper.

100 μm wires spaced 1 mm apart, the grid serves not only to support the window (which experiences a total force at 100 torr of roughly 200 lbs.) but also to minimize the dead layer between the front cathode and the foil. The grid is aligned with both cathode plane grids so as not to reduce the transmission efficiency of the PC (90%) unnecessarily.

The completed PC also incorporates the initial readout circuitry in the upper part of the PC housing. An integrated charge-sensitive pre-amp chip is AC-coupled to each of the 25 anode wires, which are commonly biased. The circuit board containing these chips is 70×30 cm in area and extends 1 cm past the housing for Lemo connections to the feedthrough cables. The board also serves to support the anode wires and direct gas flow, which proceeds first through the active area, then into the electronics housing in the upper part of the PC. Each pre-amp chip dissipates about 200 mW during operation, so the gas flow through this section is necessary to prevent overheating.
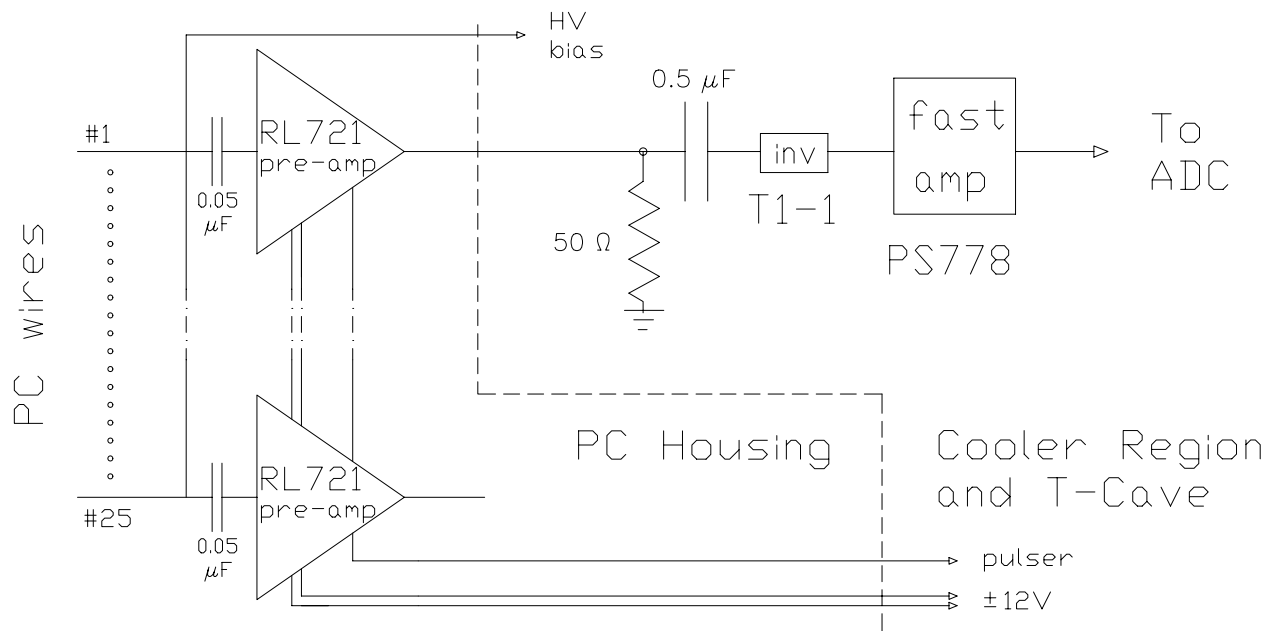

Figure 3.18   The PC electronics, for a single anode wire, as configured for the CE-06 experiment. All components shown to the left of the dashed line were enclosed inside the aluminum PC housing. Further details of the external electronics are given in Sec. 3.5.

A schematic of the readout electronics for a single wire (all wires were identically configured) is shown in Fig. 3.18. A common pulser line is bussed (along with the power) to the pre-amps for all wires, allowing complete calibration and testing of the PC readout electronics. The outputs from the pre-amps are suitable to be shaped in an amplifier or to

be fed directly into a charge-sensitive ADC. The large number of channels involved (one for each of the 25 anode wires) led to the use of the latter readout for the CE-06 experiment (cf. Sec. 3.5).

The PC was tested first at the Yale Nuclear Structure Laboratory's tandem accelerator. Here, a gold target was used to elastically scatter a ^{12}C beam at small angles into a spectrograph. The PC was placed at the focal plane of the device on a vertically moveable platform, so that the scattered ions could be directed anywhere upon the active area of the counter. Fig. 3.19 shows the energy output of two adjacent wires (4 mm apart) when the ions were directed half-way between them. Even under these conditions (high rates of $Z = 6$ ions), the wires acted as independent proportional counters. The rate of correlated events was approximately four orders of magnitude smaller than that for the uncorrelated signals, as shown in the figure, implying that there would be no ambiguity in determining the y-position.
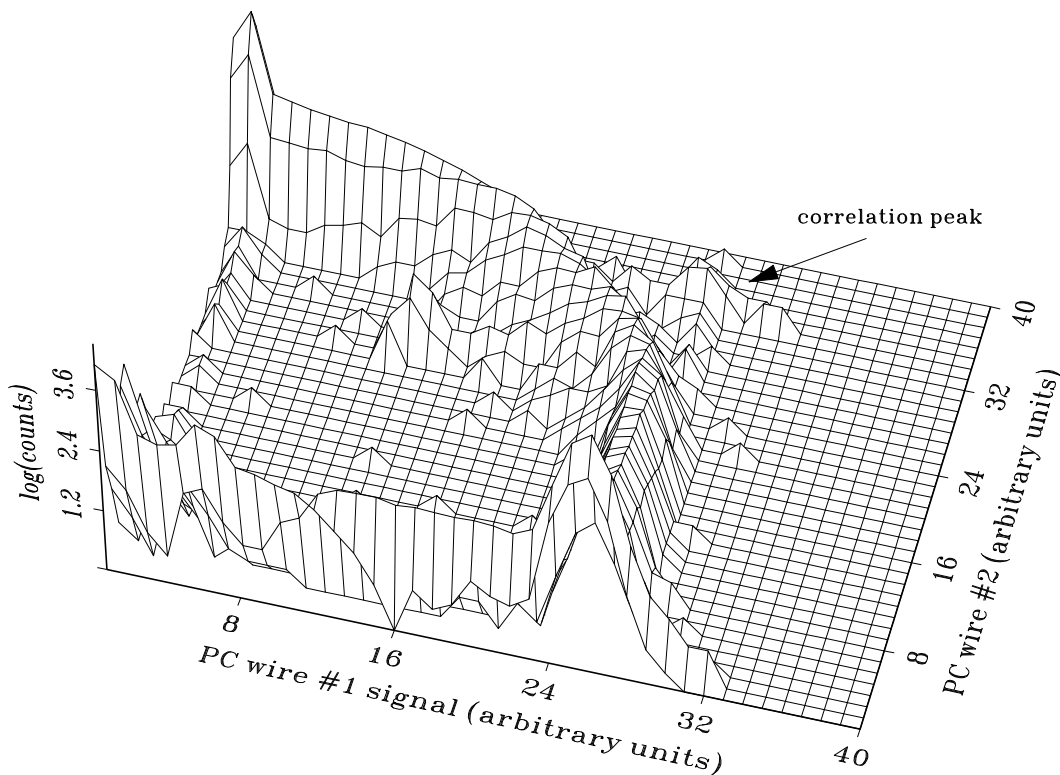

Figure 3.19   Correlation plot for adjacent PC wires with an intense stream of ^{12}C ions incident between them. The arrow points to full-energy correlated events. The vertical scale is logarithmic.

The energy resolution of the PC was determined to be approximately 6% FWHM for ions at the energy used (about 50 MeV), somewhat worse than expected from the

prototype tests. This degradation was due, as determined later (see Ch. 4), to cathode grid wires shifting slightly out-of-plane, because of a lack of tension. These shifts cause a gain variation along the length of each anode wire which, uncorrected, effectively results in poor resolution. The Yale tests also demonstrated the importance of venting the vacuum containment housing slowly, so as not to stress the thin PC foil!

Final tests of the PC were done using the Princeton Cyclotron and QDDD Spectrograph facility. The goal was to determine whether the PC was in proportional mode (and therefore whether it could properly measure Z) even at quite low pressures (below 50 torr). This was accomplished by using a 48 MeV α beam on ^{12}C, ^{13}C, and melamine to produce ^{12}C, ^{13}C, ^{13}N (from (α, t)), and ^{16}O recoils. These were selected magnetically by the spectrograph and detected by the PC at the focal plane. The tests did confirm that the PC ΔE signal for ions of the same energy was linear with Z^2 at 50 and 25 torr, although low count rates made identification difficult, especially for ^{16}O.

3.4.4 The Silicon Array

The silicon micro-strip array was the final detection element in the CE-06 detector stack. The array was used to measure an incident ion's total kinetic energy E, to provide a timing measurement for determination of the ion velocity, and to measure the ion position in the x-z plane (see Fig. 3.11). In order to eliminate the need for another foil, the detectors were to operate directly behind the back cathode grid of the PC, in the gas volume. As with the proportional counter, a large active area of at least 60×10 cm was needed to maximize the solid angle subtended to the target. To achieve this size at reasonable cost, the active area would have to be segmented as an array of smaller Si chips.

The chips used for CE-06 were built by Micron Semiconductor (England), and have an active area of 5×5 cm. The silicon wafers are attached to a custom-designed printed circuit board (PCB) for support and readout capability. A single Si chip is shown in Fig. 3.20, viewed from the front (particles are incident on this face). The particular circuit board mounting allows several chips to be placed side-by-side with minimal dead region between them.

A schematic of the internal details of one of these detectors is shown from a side view in Fig. 3.21. Each detector is a passivated, ion-implanted, n-type silicon wafer, with 50 strips (1 mm pitch) etched on the front face (see App. B for a review of solid-state detector operation). An important feature of these detectors is the thin dead layer (about 1000 Å) of evaporated aluminum on the front face. Although necessary to provide an
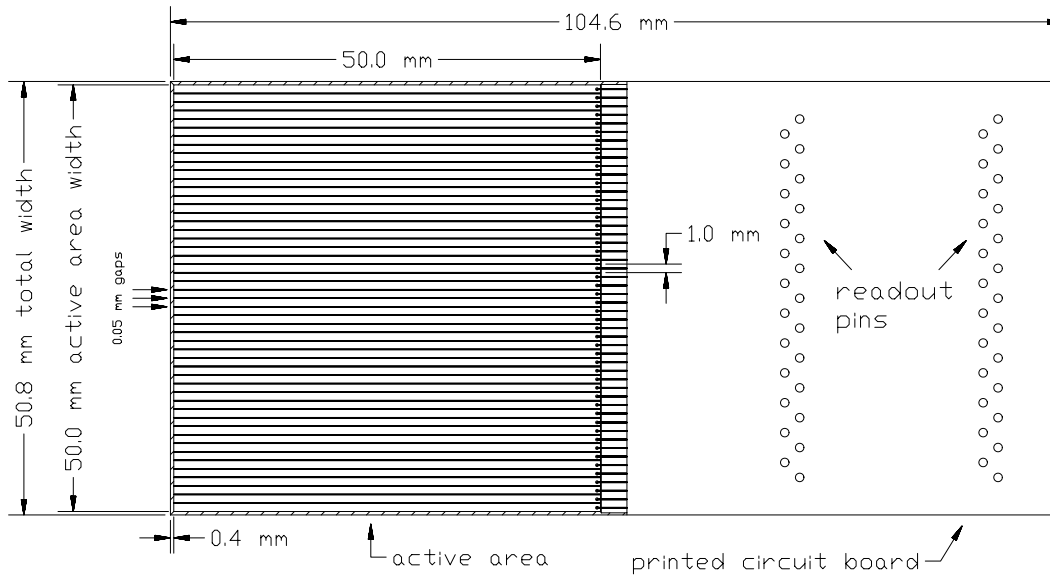
Figure 3.20   A single 5×5 cm Si detector chip. The 50 strips run parallel to the long edge of the detector The printed circuit board containing screw mount holes and pin readouts is attached at the top of the detector, for a total size of 10.5×5.1 cm.
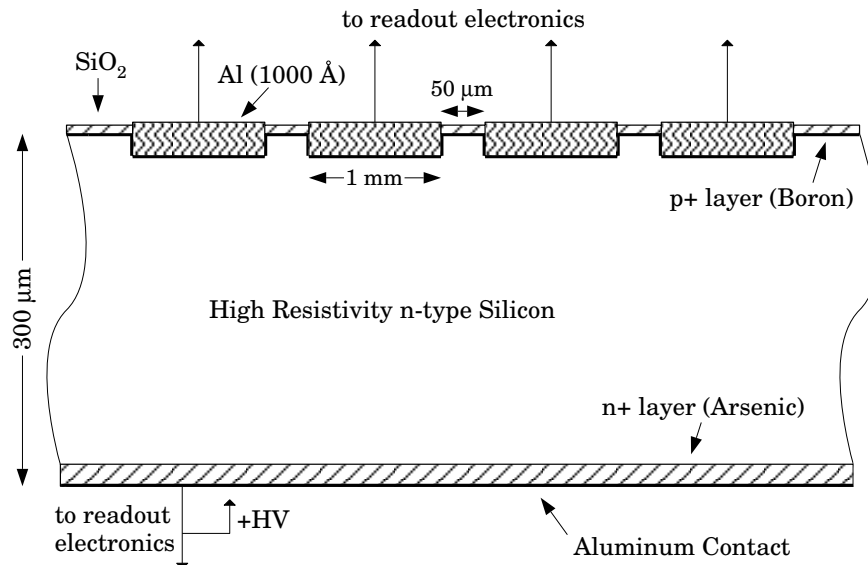

Figure 3.21   Cross-sectional view of the Si wafers used for CE-06. The layers are not drawn to scale for clarity.

electrical contact, the thinness of this layer is vital for minimization of ion energy losses.

As shown in Fig. 3.21, the chip is electrically equivalent to a p-n junction, and is fully depleted when biased by application of $V_{\text{bias}} \approx +15\,\text{V}$ to the back (the n^+ contact). The large depletion depth of 300 μm is possible because of the high-resistivity silicon used

($\rho_n \approx 20,000\,\Omega$-cm). As such, each chip is capable of stopping $Z = 6$ particles with energies up to roughly 130 MeV. The capacitance of each detector when fully depleted is roughly 1 nF.

The mounted PCB allows the readout of each strip (one pin each) and the back (one pin). In this configuration, energy and timing can be obtained from the back along with position information from the front. A significant part of the experimental development work for this project involved the construction of a readout system capable of making these three measurements simultaneously, with the following desired resolutions: $\Delta t \lesssim 1$ nsec, $\Delta E \lesssim 150$ keV, and $\Delta x = 1$ mm.
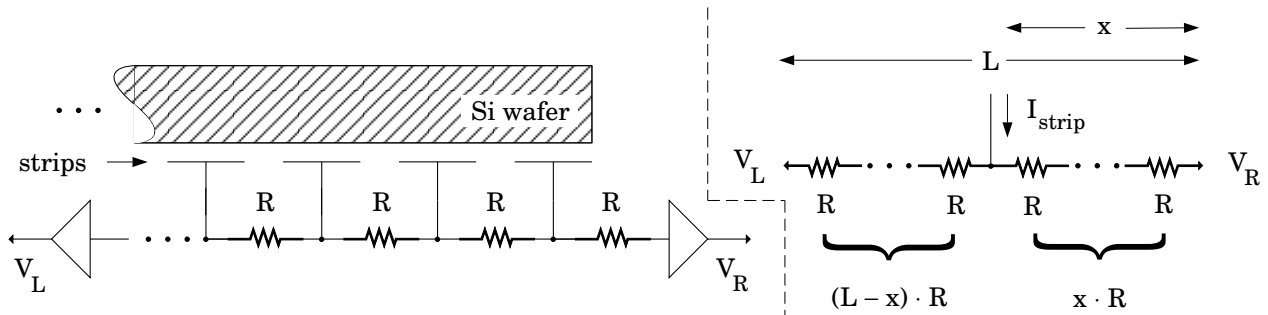

Figure 3.22 Resistive readout method for the Si detectors, shown schematically with the equivalent circuit. Tested resistor values ranged from 100–300 Ω.

Due to the large number of strips expected for the entire array (1200), and the need to have the silicon mounted inside the PC, it was desired that the position readout system would be capable of resolving each strip yet require only two position signals per chip. The first technique developed to achieve this goal employed the method of resistive charge division, shown in Fig. 3.22. A resistor chain was mounted on a chip's PCB, essentially forming a voltage divider for the current sources represented by the strips. For an ion track occurring at a distance x from the left end, the signals V_L and V_R at each end satisfy

$$x = L \cdot \frac{V_L}{V_L + V_R}, \tag{3.9}$$

where L is the chip length perpendicular to the strips.

Figure 3.23 shows the position spectrum obtained in tests with the prototype PC at the Princeton Cyclotron. Using the energy signal in place of $V_L + V_R$, a reasonable (though not complete) strip separation was obtained for an inter-strip resistance of 100 Ω. For this type of readout, higher resistor values tend to produce a better strip separation, since $\Delta V_L \propto \Delta x \cdot R$, where R is the resistor value.
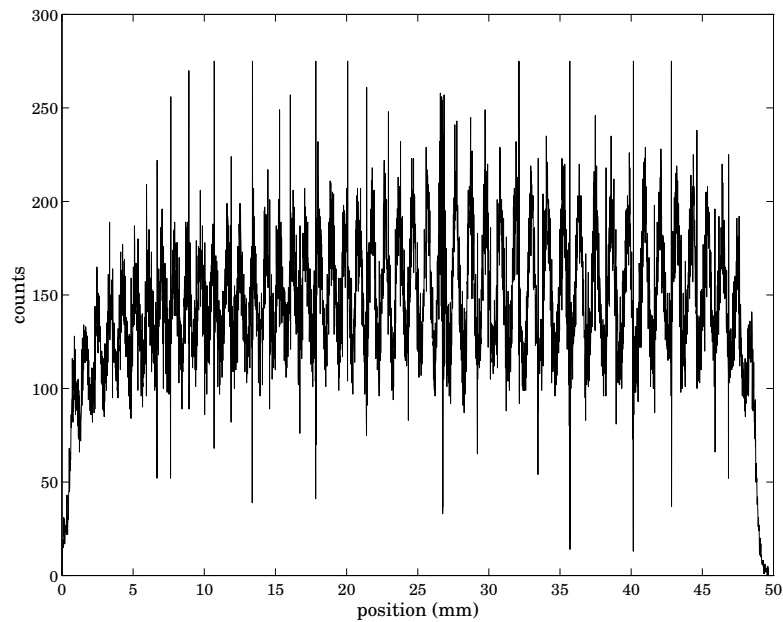
Figure 3.23   Position spectrum from a single chip illuminated by α particles with $E \approx 20$ MeV. The strip resistor value was 100 Ω, and the right end was grounded ($V_{\mathrm{R}} = 0$), so that only 49 out of 50 strips were available from the data.
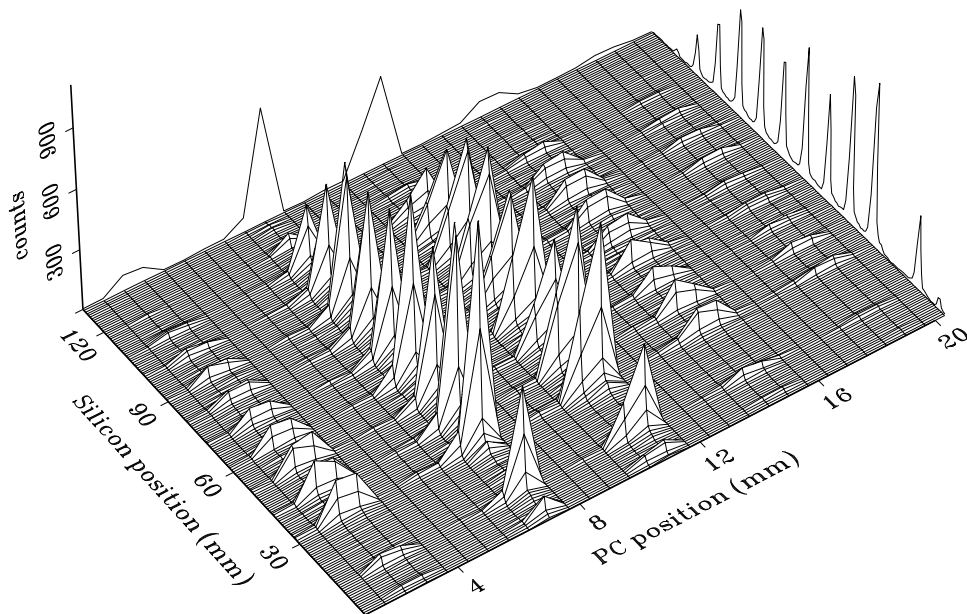

Figure 3.24   Position data for ^{12}C ions from the Yale tandem using the full-scale PC and a single 5×5 cm silicon chip, with (discrete) resolutions of 4 mm and 1 mm, respectively. One Si strip was disconnected during the test.

To test the performance of the readout method with ^{12}C ions, a chip was placed in the back of the full-scale PC for its test run at the Yale facility. Fig. 3.24 shows the two-

dimensional position information obtained by the two detectors, along with a projection of the position spectrum from the silicon. For these highly ionizing particles (50 MeV ^{12}C), each strip was clear and well-resolved from its neighbors. The energy resolution for these particles was better than 1% (about 250 keV FWHM).
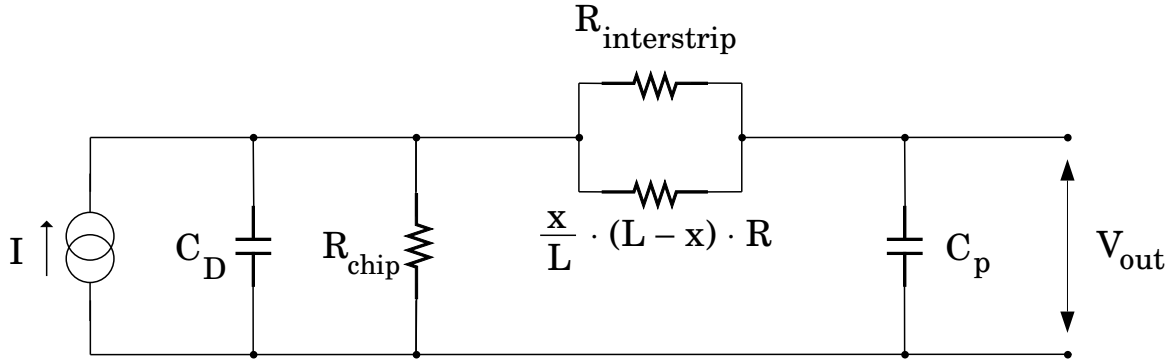

Figure 3.25   Equivalent circuit for the E_{si} and t_{si} measurements using a Si chip with resistive readout; the ionizing event is represented as a current source. C_{p} and C_{D} are the pre-amp and detector input capacitances, respectively.

These results and later data showed, however, that the timing resolution achievable which using a resistive readout was not only unacceptable ($\Delta t > 2\,\mu$sec) but highly position dependent. The equivalent circuit from the viewpoint of the timing pre-amp is given in Fig. 3.25. It can be shown that the effective risetime of the detector so configured is

$$\tau \approx RC_{\mathrm{p}}(1 - \frac{x}{L})x, \tag{3.10}$$

using the notation of Fig. 3.22. For $x = 0$ or $x = L$, the risetime is very nearly the intrinsic detector risetime (with a typical matched pre-amp capacitance) of about 25 nsec. However, for $x = L/2$, and using $100\,\Omega$ resistors, the risetime is roughly 1 μsec. Reducing the value of the resistors improves this but worsens the position resolution.

A second technique for position readout was pursued in the hope of improving the timing resolution. This method uses a delay-line configuration similar to that employed for the PGAC position readout. Fig. 3.26 shows the electronics schematic; the inductors coupled with the capacitive equivalent of each strip form a delay line with an elemental delay of $\Delta t \approx 1.5$ nsec. The left and right signals are then amplified by physically small (about 3 mm in diameter), integrated, fast pre-amp chips that could be mounted on the PCB attached to the silicon detectors. The time difference of the two position signals is proportional to the ion position (see also Eq. (3.6)), using the signal from the back as the TDC start.
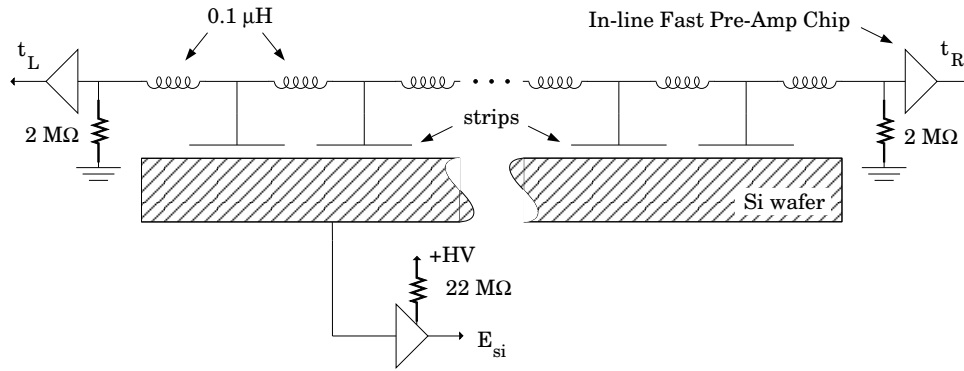
Figure 3.26   Inductive method for position readout of the Si wafers. The 0.1 μH inductors, placed between the strips (each of which is essentially a 20 pF capacitor), constitute a delay line. The small signals from each side (a few mV) are amplified by integrated pre-amp chips and discriminated.

Figure 3.27 shows α source test results of the inductive readout method. The strip separation was quite good; most of the variations in peak height per strip seen here are due to differences in the widths of the peaks. Although there were still small position variations in the timing signal risetime (mainly due to delay-line attenuation), these were quite minor compared to that associated with the resistive readout. Preliminary tests with the PGAC showed that the achievable TOF resolution was equal to or slightly better than 1 nsec.
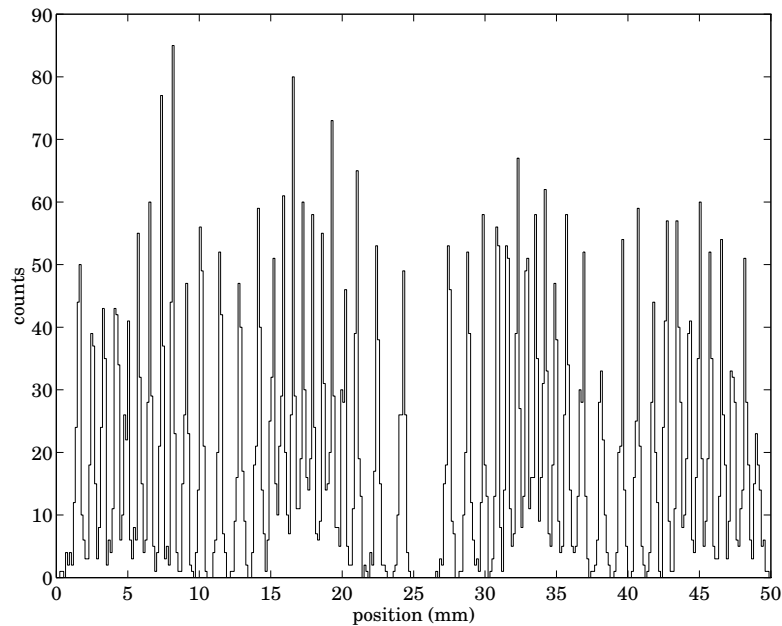

Figure 3.27   Inductive readout position spectrum for a strip detector illuminated by 8 MeV α particles. The grouping of strips (and resulting non-linearity of the strip positions) is due to the particular inductor layout on the PCB.

Unfortunately, difficulties with this readout method became apparent when the system was used with the many chips that comprised the silicon array. The problem was traced to the high-gain nature of the fast pre-amp chips designed to amplify the position signals and shape them for timing. Enough noise was generated by the chips (either radiatively or conductively through the circuit board ground plane) to be picked up by neighboring pre-amp chips via their attached silicon "antennae." The pickup would produce a self-sustaining clipping-level oscillation in the chips that would dominate any real signals. The only solution was to remove enough Si chips until the oscillation stopped, but this was untenable, since, in an actual experiment, access to the detectors would be limited due to the overhead involved in venting the vacuum enclosure.

The third technique developed for position readout, and the one actually used for the CE-06 experiment, was a return to a resistive readout with two important modifications. The first of these was a capacitive shunt to ground placed between each strip and the resistor chain (see Fig. 3.28). The effective resistance of the chain is bypassed for high frequencies by this capacitor, allowing energy/timing signal risetimes to be limited mainly by the chip's intrinsic value

$$\tau \approx \rho\epsilon \approx 25\,\text{nsec.}$$

This capacitive load also eliminates the position dependence of the risetime that was characteristic of the original resistive readout method.

The second modification was necessitated by the first: To reduce the noise contribution of the extra capacitors (totaling about 10 nF via parallel addition) to the position signal, discriminators were added to each strip before the resistor chain. This prevents the firing strip from "seeing" any of the other strips and associated capacitances. The discriminators (actually, just comparator op-amps with a stabilized threshold voltage on one input) trigger current sources located at the node points of the resistor chain, providing position dependent signals V_{L} and V_{R} as with the direct resistive readout.

Figure 3.29 shows a position spectrum for a single Si chip employing the discriminator/resistor readout method, for α particles emitted from a ^{228}Th source (see also Fig. 4.5). Complete separation (zero counts between peaks) of almost all strips is achieved, and even strips in the middle (whose discriminators see the largest series resistance) are clearly defined. Also shown in Fig. 3.29 is the corresponding timing spectrum obtained for a single chip, using the PGAC as the timing start device. The achieved resolution in this setup was $\Delta t \approx 1.3$ nsec, which, although not quite as good as that from the inductive readout, was
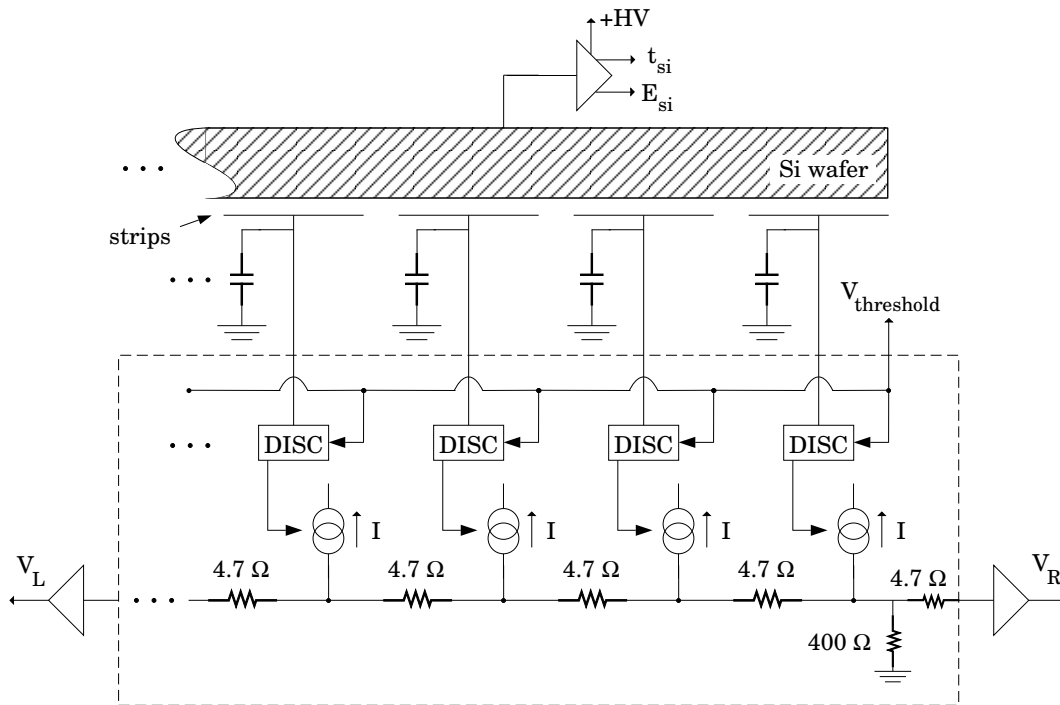
Figure 3.28 Discrimination method for position readout of the Si chips. The capacitor values are roughly 10 times the strip capacity. All the circuitry enclosed in the dotted lines was mounted on small PCBs attached to the Si wafer PCBs via short ribbon cables, for use in the restricted volume of the PC.
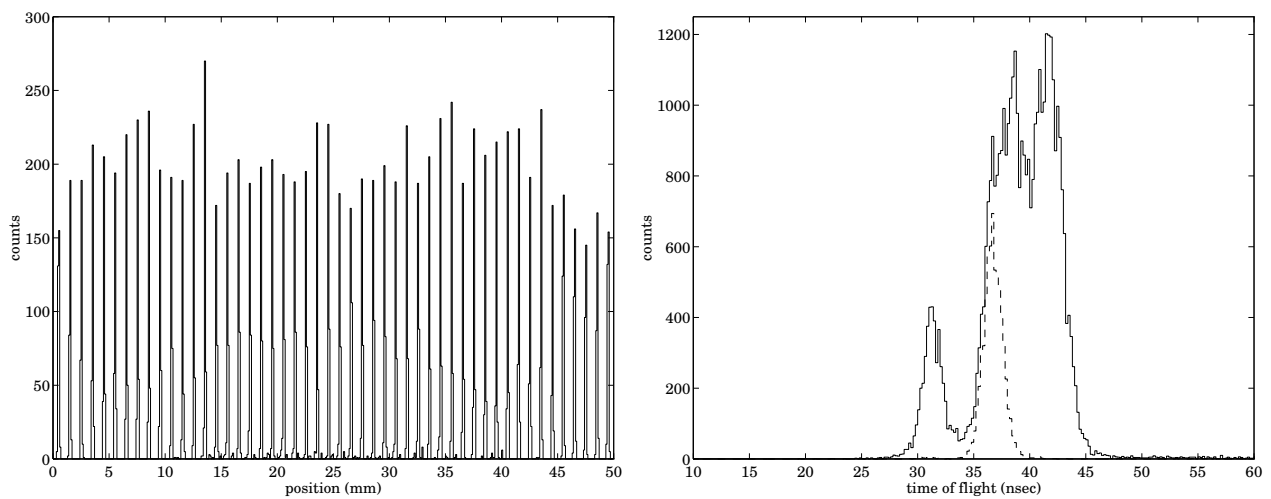

Figure 3.29 A typical position spectrum (left), using the discriminator read-out method, for 6.8 MeV α particles. Shown at right is the timing spectrum using the signal from the back of the Si wafer, illuminated by a ^{228}Th source. The dashed line indicates the unresolved 6.8 MeV peak (FWHM $\approx$ 1.3 nsec).

within the range of acceptability. The energy resolution using this method was typically $\Delta E \approx 150$ keV, for 8 MeV α particles.
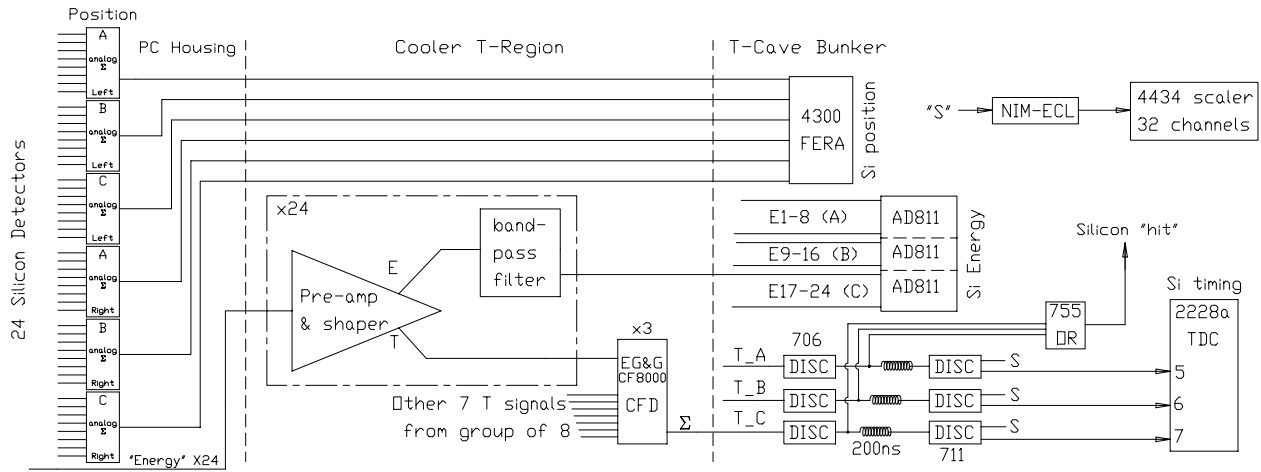
Figure 3.30   The Si electronics used in the CE-06 experiment. Physical locations are delineated by the dashed lines (see Fig. 3.31 below). Sec. 3.5 gives further details of the bunker electronics.

A ramification of such a readout system is the need (for the purpose of this work) to use 1200 discriminators, one for each strip, close to the detectors. To accomplish this, a low-power, small-sized discriminator circuit board was developed [Ho93], enabling the operation of the discriminator electronics for 24 silicon chips in the back of the PC, whether in gas or vacuum. Figure 3.30 shows the CE-06 electronics configuration for readout of the silicon array. To reduce the number of feedthroughs, the position signals were analog-multiplexed into three groups of eight signals each for "left" and "right." Determining the detector that fired could then be handled in software by setting appropriate conditions on the (non-multiplexed) energy signals.
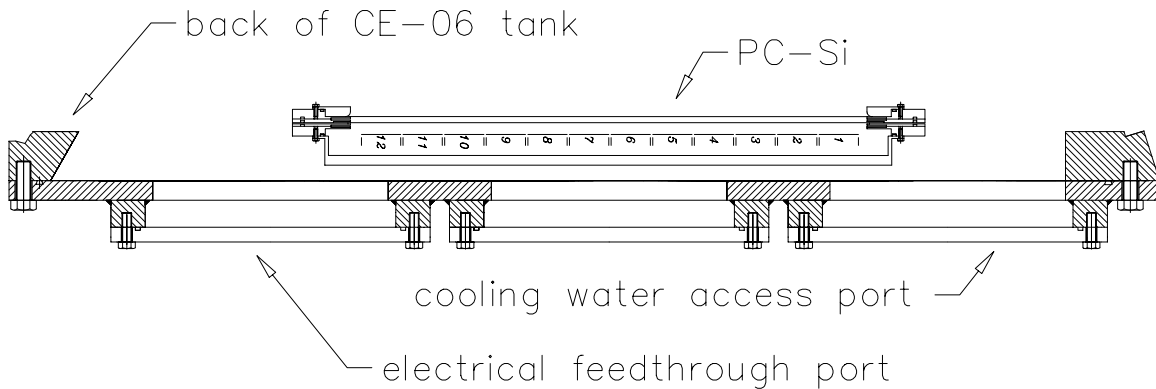

Figure 3.31   The PC and Si detector array assembly, as used in this work. Ions are incident from the top of the figure.

Figure 3.31 shows the physical setup for the PC-Si detector assembly in place as used

for the CE-06 experiment. The unit was mounted near the back of the vacuum tank (see Fig. 3.9), with electrical feedthroughs connected to one the back tank ports. Directly outside the ports were pre-amp/shapers (one for each Si chip) to construct the energy and timing signals, the latter which were then OR'd (by three eight-channel discriminator modules) into three signals corresponding to the position signal groupings. To allow use of the position readout even while in vacuum (no gas in the PC), and to improve the Si detector energy resolution, water at $0\,^\circ$C was pumped through copper tubing thermally attached to the back of the PC.

3.4.5 The Luminosity Monitor

Although not formally part of the CE-06 detector stack, the luminosity monitor detector system was an important component of the experiment. In a single-pass accelerator experiment, the beam current can be measured fairly accurately using a Faraday Cup beam dump or by other direct means. Clearly, however, any method to measure I_{beam} that disturbs the beam in a significant manner is not suitable to the Cooler ring.
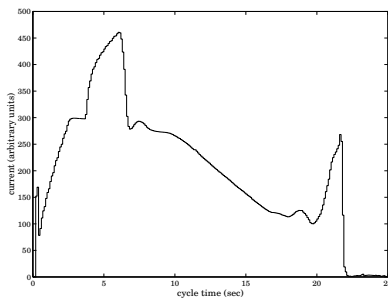

Figure 3.32 I_{ring} vs. t (sec).

Inductive measuring devices have been developed but are not completely reliable for measuring current at the desired level (accurate to a few percent for currents of less than 1 mA). The figure at left shows a typical on-line spectrum of one of these devices, installed on the Cooler ring, for a CE-06 cycle (current in arbitrary units). Problems are especially apparent at the low beam currents (typically, 50–100 μA) near the end of the cycle where the device (falsely) shows an increase in current (for comparison, see Fig. 3.3).

Another factor in the luminosity determination is the target thickness, which can often be determined fairly precisely for a self-supporting target. For the very thin targets used in the Cooler, however, a direct thickness measurement can be very difficult or nearly impossible (as in the case of a gas jet target or a target such as a fiber that doesn't cover the entire beam). In this situation, the most accurate way to measure the luminosity is to determine the event rate for a known (and large) cross-section for a process that is concurrent with the reaction under study.

Figure 3.33 shows the luminosity monitor setup used for the CE-06 experiment. The monitor was comprised of two main parts. The first of these was a Si detector (a 5×5
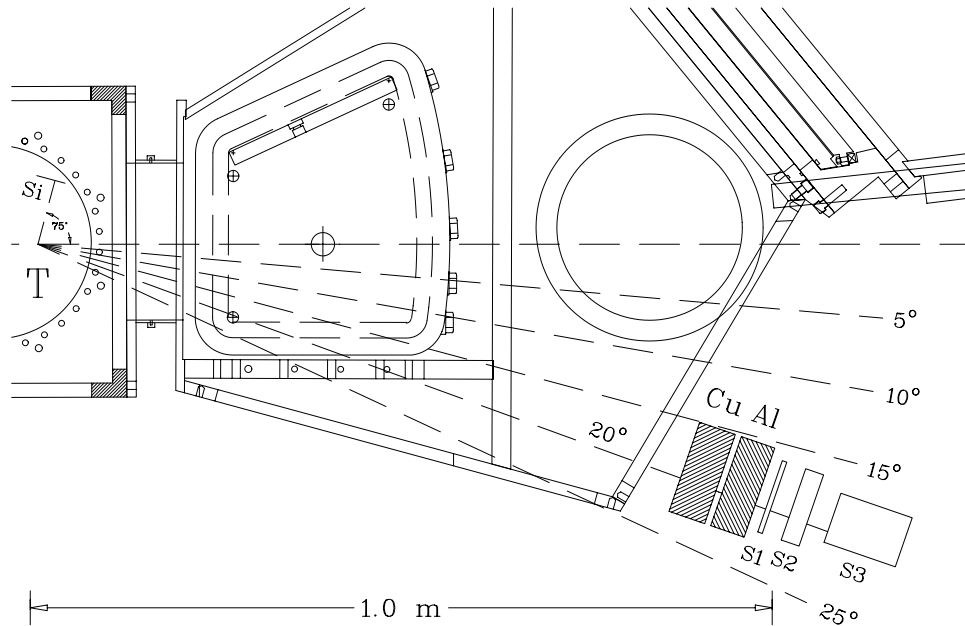
Figure 3.33   Luminosity monitor system for the CE-06 experiment. Shown is the configuration of the monitor for $E_p = 330$ MeV as used in the February, 1993 production run.

cm chip identical to those in the main array) mounted at the beam height less than 10 cm from the target-beam interaction point, located at 75° to the beam direction. The second component was a set of three scintillators, directly preceded by absorbers, mounted just outside the magnet box and centered at 19° degrees with respect to the beam. For $E_p = 330$ MeV, the absorbers consisted of copper and aluminum slabs, 2.0 and 1.88 inches thick, respectively. The scintillator thicknesses for S1, S2 and S3 (see Fig. 3.33) at this beam energy were 0.25, 1.0, and 4.0 inches, respectively.

With this system, the luminosity is measured by determining the number of events from $^{12}C(p, p')^{12}C^*$, where the ^{12}C ground state and first excited state are primarily populated. Since the cross-section for this process is fairly well-known (see [Js86] and [Me83], e.g.), the time-averaged luminosity can be found by inverting

$$N = L_{\text{ave}} \cdot \left[\int_{\Delta\Omega} \frac{d\sigma}{d\Omega} \, d\Omega \right] \cdot \Delta t, \tag{3.11}$$

where N is the total number of monitor events. For this setup, the scintillator defines the acceptance and therefore the limits of integration. The recoil ^{12}C ions can be detected in the Si monitor, in coincidence with a proton event in the scintillators, for the most precise determination of N.

In practice, this coincidence rate is difficult to measure due to the low energy (a few MeV) of the recoils and the relatively high noise-level associated with operating a high-capacitance detector mounted close to the beam. By careful adjustment of the absorber thicknesses, however, a reliable identification of the elastic and inelastic protons scattered from the target can be made by measuring dE/dx and E. The absorbers allow the final scintillator to stop the proton, and ensure a reasonable signal size in the transmission scintillators. The angle of the scintillators with respect to the beam, $\theta \approx 20°$ as run in CE-06, was made large enough to avoid any small-angle multiple scatterings in the target, while maintaining a reasonable event rate (the cross-section for proton scattering drops off steeply for the beam energies used in CE-06).

3.5 Electronics

The complete electronics used for the CE-06 final production runs of December, 1992, and February, 1993, are shown in Figs. 3.13, 3.18, 3.30, and 3.34. Central to the logic scheme shown in the latter figure was the Bira 2206 CAMAC module. This component allowed simultaneous acquisition of several event streams, each involving different CAMAC readout schemes, of various readout priorities. Scalar events (Bira #4) occurred throughout the runs every 0.1 sec (artificially produced by a clock), and consisted of readouts of several detector rate counters (denoted by "S" in the figure). The data was stored in a single-width 32-channel LeCroy 4434 scaler module, for efficient block readout.

A detector stack event (Bira #6) consisted of a coincidence between the PGAC and any one of the silicon detectors. The twenty-four silicon detectors were multiplexed into three groups of eight detectors each, for the position and timing signals. Even so, event #6 required the readout of 55 linear signals (twenty-five for the PC ΔE signals, twenty-four for the silicon detector E signals, and six for silicon position) and 11 timing channels (three for the silicon and eight for PGAC position and timing). Although this total number could have been greatly reduced with a hardware logic trigger and fast clear, the fairly significant gain corrections needed for gain matching of the PC wires and Si chips were possible to carry out only at the software level and so it was necessary to readout all possible channels.

To accomplish the readout, LeCroy 4300B FERA modules were used for fast conversion (in less than 10 μsec) of the linear and timing signals (the latter in conjunction with 4303 TFC modules). These were readout in zero-suppression block mode, leaving the relatively slow AD811 ADC modules (80 μsec conversion) for the E signals last in the
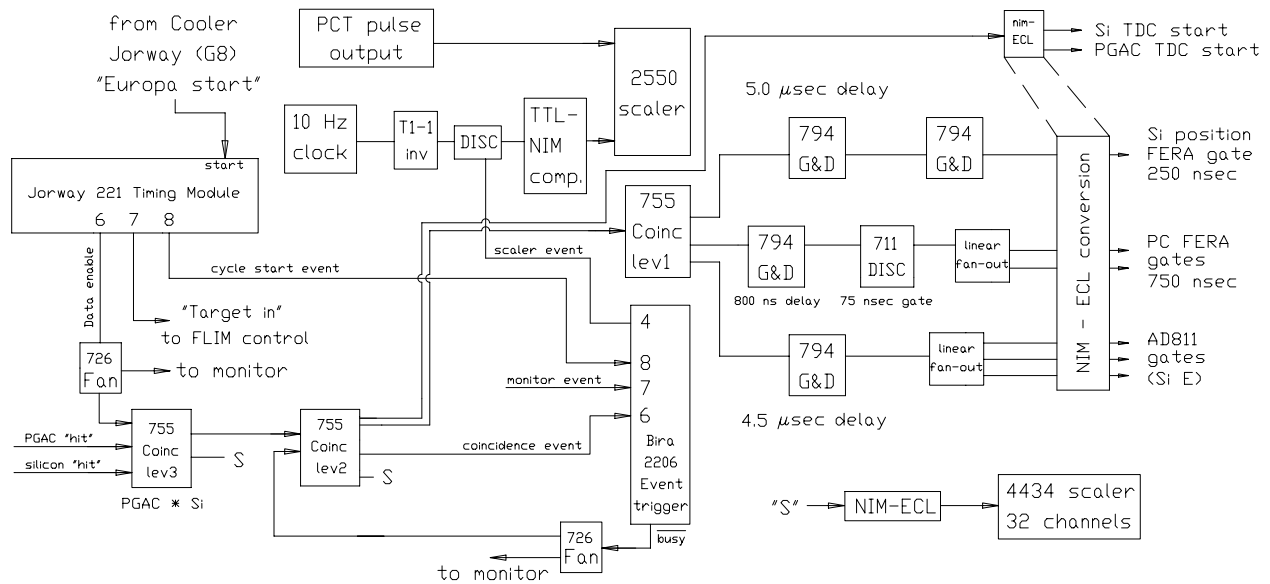
Figure 3.34   Electronics logic configuration for the final CE-06 run. The
PGAC and Si "hit" signals were generated via the electronics of Figs. 3.13 and
3.30, respectively. The luminosity monitor electronics are not shown.

readout process. In this way, hardware readout rates for the event #6 stream of roughly
1 kHz were easily attained for direct writing to tape (with no computer processing).

As a separate Bira event stream (#7), the monitor detectors were readout upon receipt
of a coincidence trigger from two of the proton arm scintillators. The silicon monitor was
readout in slow coincidence with this trigger, since the expected slow rate of true luminosity
^{12}C-p coincidence events (on the order of 1 Hz) suggested that a software coincidence
measurement would be a reasonable choice. However, the sensitivity to protons made this
event stream the most active one during the CE-06 production runs.

Event stream #8 was an artificial event corresponding to the beginning of each Cooler
cycle (the trigger was obtained from the ring's ramping computer). At an appropriate time
later (soon after the receipt of another signal, "Cooler Ready"), the target would be moved
into the beam. All such times in the cycle period pertinent to the experiment were stored
in the Jorway 221 module (near the upper left of Fig. 3.34), which provided a logical "true"
when that time was reached. In this way data was taken only when the beam was properly
cooled and the target was in position. This "data-on" time ranged from roughly 10 to
25 sec depending on the beam current and lifetime with the particular target.

The only major readout difficulty concerned the PC. Since the internal PC pre-amps
invert their (negative) input signals, the signals must once again be inverted and atten-
uated to be used with the FERA modules, which are sensitive to negative input charge.

Integrated, passive transformer chips were used as inverters, preceded by high-pass filters (characterized by $(RC)^{-1/2} \approx 200$ Hz) for AC coupling and reduction of 60 Hz noise induced by the long ground cable leads from the T-Cave area to the T-Site. An extra resistor was used in each wire's circuit as part of a resistive divider in order to provide an attenuation by a factor of two. This kept the charge integration of the slow PC pre-amp output signals (with fall times of approximately 10 μsec into 50 Ω) below the FERA saturation limit of $Q_{\mathrm{max}} \approx 480$ pC.

A fast amplifier for each channel was necessary since the PC had to be run at a relatively low voltage ($V \approx +565$ volts compared to the prototype voltages of 800–1000 volts). This reduction served not only to reduce the output signal size so as not to produce FERA overflows, but also to minimize gain variations due to the non-rigid cathode grids. Without the amplifier stage, the signal-to-noise ratio was unacceptably small (about 4:1) under these conditions, so twenty-five channels of fast amplifiers, at or near the lowest gain settings, were used for most of the production runs.